Wireless Information and Power Transfer Methods for IoT Applications

Ryan Reed

Thesis submitted to the faculty of the Virginia Polytechnic Institute and State University in partial fulfillment of the requirements for the degree of

Master of Science

In

Electrical Engineering

Dong Sam Ha, Chair

Cindy Yi

Arthur H. Ball

June 9th 2021

Blacksburg, Virginia

Keywords: Wireless power transfer, RF energy harvesting, Internet of Things

Wireless Information and Power Transfer Methods for IoT Applications

Ryan Reed

ABSTRACT

As Internet of Things (IoT) technology continues to become more common place, demand for self-sustainable and low power networking schemes has increased. Future IoT devices will require a ubiquitous energy source and will need to be capable of low power communication. RF energy can be harvested through ambient or dedicated RF sources to satisfy this energy demand. In addition, these RF signals can be modified to convey information. This thesis surveys a variety of RF energy harvesting methods. A new low complexity energy harvesting system (circuit and antenna) is proposed. Low power communication schemes are examined, and low complexity and efficient transmitter designs are developed that utilize RF backscattering, harmonics, and intermodulation products. These communication schemes operate with minimal power consumption and can be powered solely from harvested RF energy. The RF energy harvester and RF powered transmitters designs are validated through simulation, prototyping, and measurements. The results are compared to the performance of state-of-the-art devices described in the literature.

Wireless Information and Power Transfer Methods for IoT Applications

Ryan Reed

GENERAL AUDIENCE ABSTRACT

Future devices are expected to feature high levels of interconnectivity and have long lifetimes. RF energy from dedicated power beacons or ambient sources, such as Wi-Fi, cellular, DTV, or radio stations can be used to power these devices allowing them to be battery-less. These devices that harvest the RF energy can use that energy to transmit information. This thesis develops various methods to harvest RF energy and use this energy to transmit information as efficiently as possible. The designs are verified through simulation and experimental results.

Acknowledgements

Thank you to my advisor, Dr. Dong S. Ha, for his support, enthusiasm, and leadership. Throughout my graduate study, Dr Ha worked hard to ensure I was getting the proper resources and guidance to succeed. His energy and personality also made the Multifunctional Integrated and Circuits and Systems (MICS) group an enjoyable place to work. I also want to thank Dr. Cindy Yi and Dr. Arthur Ball for serving on my committee and knowledge they have provided me with as instructors.

I would not be able to succeed without the support of my peers in the MICS lab: Jinhua Wang, Fabiha Nowshin, Fairborz Lohrabi Pour, Rajesh Kudupudi, Kang Jun Bai, Jiayu Li, Junjie Wang, Yibin Liang, Hongyu An, Abhishek Damle, Xingye Liu, Shiya Liu, Jiayuan Zhang, Moqi Zhang, Victor Gan, Long Huang, and Keyvan Ramezanpour. Their eagerness and assistance made MICS a friendly learning environment. I wish you all success in the future.

Finally, I thank God for his presence and guiding me to success. I am grateful to have the support of great friends. I also appreciate the support of my father, Jeffrey Reed, my mother, Pamela Reed, and my sister, Julia Reed.

Table of Contents

List of Figures

List of Abbreviations

SWIPT	Simultaneous wireless information and power transfer
RF EH	RF energy harvesting
IoT	Internet of Things
WSN	Wireless sensor nodes
WPT	Wireless power transfer
PCE	Power conversion efficiency
IMN	Input matching network
OMN	Output matching network
HWD	Half wave dipole
LOS	Line of sight propagation
WPT TX	Wireless power transfer transmitter
PSD	Power spectrum density
IF	Intermediate frequency
ISM	Industrial, scientific, and medical
HEMT	High electron mobility transistor
ASK	Amplitude shift keying
VCO	Voltage controlled oscillator

Chapter 1: Introduction

1.1 Motivation

The development of Internet of Things (IoT) technology has resulted in large scale networks that are typically composed of numerous wireless sensor nodes (WSN). Many of these devices are intended to have long lifetimes, high portability, or be implemented in secluded areas. These constraints make conventional sources of energy, such as batteries, impractical. Furthermore, traditional RF circuits consume a significant amount of power making them ill-suited IoT networking schemes. Because of these challenges, new methods for simultaneous wireless information and power transfer (SWIPT) have become an emerging research topic.

RF energy harvesting (RF EH) and wireless power transfer (WPT) technologies are key components in SWIPT systems. RF EH converts ambient RF energy from sources such as FM & AM radio stations [1]-[3], DTV [4]-[5], cellular networks [6]-[9], and 2.4 GHz ISM band transmissions [10]-[12] to usable DC. In contrast, WPT systems feature a dedicated power transmitter called a power beacon. Both technologies allow for far field transfer of power and can power numerous devices in a wide area.

Along with providing power, RF signals can also convey information to remote devices. These devices operate using only harvested RF power so they must be very power efficient. Low power devices can leverage RF backscattering or harmonics generated by electronic circuitry for efficient communications. Each of these methods has its own advantages as well as disadvantages and will be discussed in this work.

1.2 Scope of the Proposed Research

The structure of a typical SWIPT system is shown in Figure 1.1. Each device or tag contains an energy harvester, which can receive energy from a dedicated power transmitter or an ambient source. It uses this energy to power a microcontroller which can read information from a sensor node and convey this information through a simple transmitter. The transmitted information is then received by a base station or another tag to form large networks.

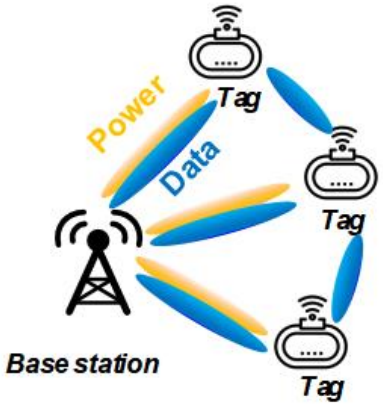

Figure 1-1: SWIPT network structure.

As the complete design of a SWIPT network can be very complicated, this work is primarily focused on the tag and power transmitter design. For the tag design, the goal is to develop an energy harvester with the ability to harvest as much energy as possible. To do this, the developed system needs to efficiently receive as much RF energy as possible and feature a high RF-to-DC power conversion efficiency (PCE). The tag must also be able to convey information with minimal power. To be practical, the power transmitter should consume minimal power while transmitting sufficient RF energy so that the tag can function property. Minimizing the power transmitter radiated energy can also reduce the probability of causing interference.

1.3 Proposed Approach and Technical Contributions

The proposed tag features an energy harvester that maximizes DC power at the output by incorporating multiple antennas and using an efficient RF-to-DC rectifier. The rectifier achieves a high PCE by using a differential topology and eliminating a power combiner at the input. The harvested energy is used to power a microcontroller that can be used to control a transmitter on the tag. Two transmission methods, one that uses RF backscattering and another that uses harmonics generated by the rectifier, are proposed. The advantages for each scheme and design trade-offs are also discussed. The designs are verified through simulation and experimental results.

A multitone power transmitter is also designed to showcase WPT applications and advantages over ambient RF EH. The power transmitter uses a harmonic feedback oscillator with a diplexer to extract both the fundamental and second harmonic signals at a high-power level. A procedure for optimizing the transmitter and tag design is developed using simulation results.

The most significant contributions of this work are the developed high PCE RF energy harvester, high bit-rate backscattering communication system, and the proposed harmonic extraction SWIPT system.

1.4 Organization of this Thesis

The organization of this thesis is as follows. Chapter 2 describes the necessary background information needed to understand wireless power and information transfer. This chapter discusses the principles behind RF fundamentals such as S-parameters, antenna characteristics, signal propagation, and link budgets. The basic principles of RF EH, transmitter architecture, backscattering, and harmonic extraction are also discussed. Chapter 3 presents the design and experimental validation for a RF energy harvesting system. Chapter 4 extends wireless energy transfer to the design of a RF powered backscatter modulator. The experimental and simulation results for a backscatter tag are provided. Chapter 5 presents a dedicated RF power transmitter that utilizes two tones to enhance energy harvesting at the tag and relay information. Chapter 6 concludes the work and discusses the impact of the research and future directions.

Chapter 2: Preliminaries

This chapter introduces the key background knowledge needed to understand the contributions of this thesis. Section 2.1 provides a brief overview of concepts and definitions relevant to wireless power and information transfer. Section 2.2 explains the general operation of a RF energy harvester and examines previous works. Section 2.3 discusses the implementation of a dedicated RF wireless power transmitter. Section 2.4 deals with low power communication methods that can be utilized by wireless sensor nodes for IoT applications. Lastly, section 2.5 summarizes the chapter.

2.1 RF Definitions and Concepts

2.1.1 S parameters, Impedance Matching, and Transmission Lines

Because of their ease to measure at high frequencies, S parameters are commonly used to measure circuit networks at high frequencies. A typical N port network is shown in figure 2.1 and the matrix representation is given in equation 1 [15].

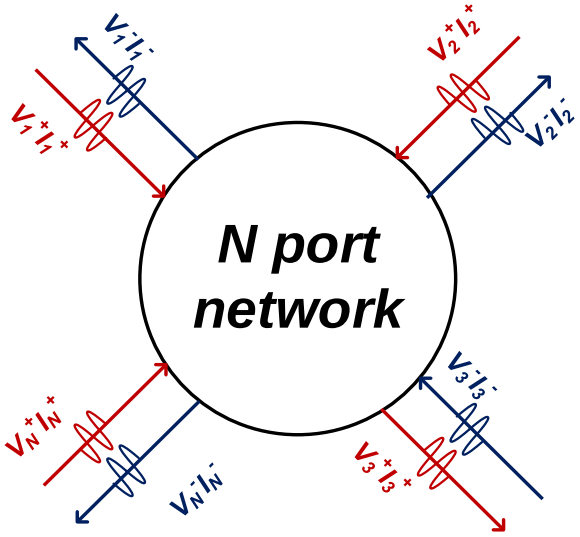

Figure 2-1: N port network.

$$\begin{bmatrix} V_1^- \\ V_2^- \\ \vdots \\ V_N^- \end{bmatrix} = \begin{bmatrix} S_{11} & S_{12} & \dots & S_{1N} \\ \vdots & \vdots & \vdots & \vdots \\ \vdots & \vdots & \vdots & \vdots \\ S_{N1} & S_{N2} & \dots & S_{NN} \end{bmatrix} \begin{bmatrix} V_1^+ \\ V_2^+ \\ \vdots \\ V_N^+ \end{bmatrix} \quad (1)$$

A specific S parameter can be determined as

$$S_{ij} = \left.\frac{V_i^-}{V_j^+}\right|_{V_k^+=0\ for\ k\neq j} \tag{2}$$

where *i* represents a specific row and *j* represents a specific column. For a simple two port network the *S* matrix can be expressed as

$$S = \begin{bmatrix} \frac{V_1^-}{V_1^+} & \frac{V_1^-}{V_2^+} \\ \frac{V_2^-}{V_1^+} & \frac{V_2^-}{V_2^+} \end{bmatrix} \tag{3}$$

$$S_{11} = \frac{V_1^-}{V_1^+}\ S_{12} = \frac{V_1^-}{V_2^+}\ S_{21} = \frac{V_2^-}{V_1^+}\ S_{22} = \frac{V_2^-}{V_2^+}$$

S – parameters are also useful in RF design as they have physical interpretation [16]. An example for a two-port network is given in the table 2-1 below.

Table 2-1: Physical interprertation of S parameters for a two-port.

Parameter	Physical meaning
S_{11}	Input voltage reflection coefficient, Γ_i
S_{21}	Voltage transfer coefficient from port 2 to port 1
S_{12}	Voltage transfer coefficient from port 1 to port 2
S_{22}	Output voltage reflection coefficient, Γ_o

In this work S parameters will be used to validate the design of impedance matching networks. Impedance matching is a vital concept in RF circuit design and can be used for stability, gain, and maximining power transfer [16]. Maximum power is delivered when the load impedance is conjugately matched to the source impedance. For matching between real-to-real passive impedances, this occurs when reflection, S_{11}, is minimal and the forward voltage gain, S_{21}, is equal to zero. At high frequencies it is useful to use transmission lines, connections that are comparative in length to the wavelength of the signal, as impedance matching networks. This is because lumped elements such as discrete capacitors and inductors are difficult to realize at high frequencies. Transmission lines must also be considered when routing the traces to avoid unwanted reflections.

2.1.2 Antenna Directivity and Gain

Antennas are used in SWIPT systems to transmit energy and information. In RF energy harvesting systems, they act as the transducer, converting received electromagnetic energy into electrical energy.

Directivity is an important parameter used to characterize an antenna. It describes the maximum radiation intensity in the main beam to the average radiation intensity in all directions [17]. It can be determined using the equation below where $U(\theta, \phi)$ represents the radiation intensity of the radiated electromagnetic field as a function of the elevation angle, θ, and azimuth angle, ϕ [17].

$$D = \frac{4\pi U_{max}}{\int_{\theta=0}^{\pi} \int_{\phi=0}^{2\pi} U(\theta, \phi) \sin(\theta)\, d\theta d\phi} \tag{4}$$

A theoretical antenna that radiates equally in all directions is called an isotropic antenna and has a radiation intensity $U(\theta, \phi) = 1$ and the directivity is computed to be 1 or 0 dB using the equation above. Because the directivity of an isotropic radiator represents the absolute minimum, directivity is often expressed relative to an isotropic source with units dBi [17].

Antenna gain considers the directivity and losses in an antenna. It is computed using the equation below where $\epsilon_{antenna}$ represents the radiation efficiency. The antenna gain is always less than the directivity. This work uses patch antennas for their ease of implementation on a printed circuit board (PCB); these antennas typically exhibit a radiation efficiency of ~70%.

$$Gain = \epsilon_{antenna}\, D \tag{5}$$

2.1.3 RF Links and Propagation Fundamentals

A transmitted RF signal can be greatly modified depending on its characteristics or the surrounding environment. Free space propagation is one of the simplest situations in which there is a line-of-sight (LOS) link between the transmitter and receiver and there is negligible reflection, scattering, or diffraction [17]. The Friis equation shown in (6) describes the power received by a receiver for free space propagation [16]. In this equation, P_R and P_T represent the received power and transmitted power, G_R and G_T represent the receive and transmit antenna

gains, R represents the distance between the transmitter and receiver and λ represents the wavelength of the signal.

$$P_R = P_T G_T G_R \left(\frac{c}{4\pi R f}\right)^2 \tag{6}$$

The Friis equation is more commonly written in decibel form [17].

$$P_R(dB) = G_R(dB) + G_t(dB) + P_t(dB) - 10\log\left(\frac{4\pi R c}{f}\right)^2 \tag{7}$$

While LOS propagation is not applicable to numerous wireless power transfer and RF EH scenarios, the Friis equation can be useful to extract general trends that will be explained in later sections.

2.2 RF Energy Harvesting Overview

The general structure of a wireless energy harvester is shown in figure 2-2. It consists of an antenna to receive the ambient or dedicated RF power source, an impedance matching network to maximize power transfer, a rectifier to convert the RF signal into a DC signal, and a DC load or storage device. The complete energy harvesting receiver is commonly called a rectenna and its design is heavily dependent on the received RF source and its power level. This section examines how these two parameters influence the rectenna design.

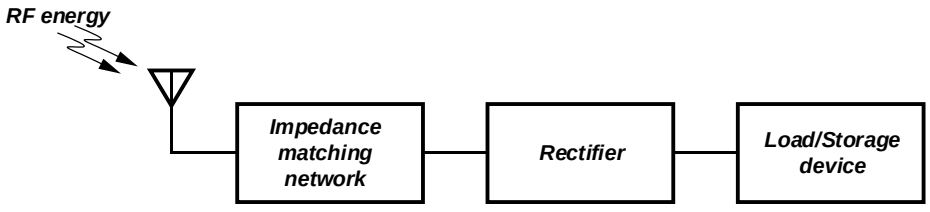

Figure 2-2: Typical RF energy harvester.

2.2.1 RF EH Sources

There are numerous frequency bands RF energy harvesters can use as an energy source. Each RF source has a unique transmit power, frequency, and availability. Table 2-2 shows typical RF energy harvesting sources and their associated characteristics. The 2.4 GHz ISM band in the table encompasses commonly used signals such as WiFi and Bluetooth. It is important to note that

the power density for each RF source is heavily dependent on location and can change significantly if the rectenna operates indoors or outdoors.

Table 2-2 RF EH sources

Source	Works	Frequency (MHz) [4]	Transmit Power (W) [18] [19]	Typical Power Density ($\frac{nW}{cm^2}$) [4] [18]
FM stations	[1] – [3]	88 – 108	≥10kW	5.59
DTV	[4]-[5]	470-512	≥10kW	10.6
GSM 900	[6]-[9]	925 – 960	≈ 8 W	36
GSM 1800	[6] – [9]	1710-1880	≈ 4 W	.5
2.4 GHz ISM devices	[10] – [12]	2400-2500	< 1 W	.18

For some RF EH applications the received power can be increased is by increasing the gain of the antenna. This allows the antenna to concentrate more of its radiation power in a particular direction at the expense of narrowing the antennas beamwidth. Increasing the antenna gain is useful in applications where the RF source is known.

The size of the rectenna system also depends on the RF source. As low frequencies result in a large wavelength, the antenna size must increase. For example, a half wave dipole (HWD) antenna for harvesting energy at the 2.4 GHz ISM band would be ~6.25 cm long while the length for a FM station antenna would be ~150 cm. The compactness and availability of the 2.4 GHZ ISM band makes it attractive for IoT applications despite its relatively low power density.

2.2.2 RF EH Voltage Doubler

Because of the low received power levels, it is vital that the rectification circuit provide a high RF-to-DC power conversion efficiency. There have been numerous RF-to-DC rectifier topologies proposed in literature. One of the most effective and common topologies used is the voltage doubler which is shown in figure 2-3 [20].

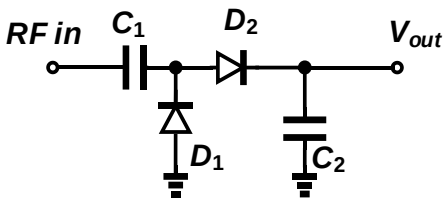

Figure 2-3: Voltage doubler.

The voltage doubler operation is simple and allows for a high DC output voltage. Assuming ideal diodes the capacitor C_1 is charged to the peak amplitude V_i during the negative clock voltage cycle. Then, during the positive, the capacitator C_2 is charged to $2V_i$. The negative and positive voltage cycles are given in figure 2-4 and 2-5 respectively.

The threshold voltage of the diodes along with the diodes conduction resistance and saturation current are critical components that determine the performance of the rectifier [21].

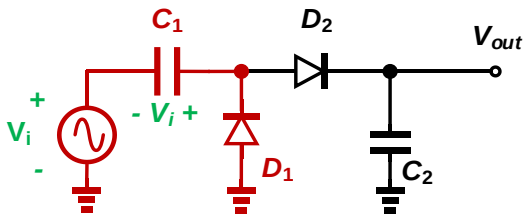

Figure 2-4: Operation of voltage doubler during negative voltage cycle.

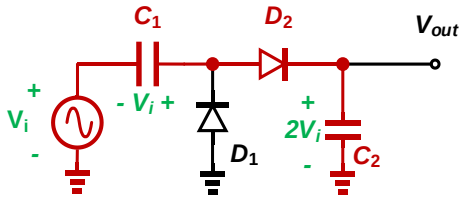

Figure 2-5: Operation of voltage doubler during positive cycle.

2.3 **Wireless Power and Information Transfer**

The low power density provided by ambient sources is not sufficient for some IoT applications. To address this, dedicated base stations have been developed to wirelessly supply energy to IoT devices. These IoT devices are often called a tag and can rely on information which can be received by the base station or another tag. A block diagram of a SWIPT system is shown

in figure 2-6. This section examines the transmitter and tag architectures and criteria to measure their performance.

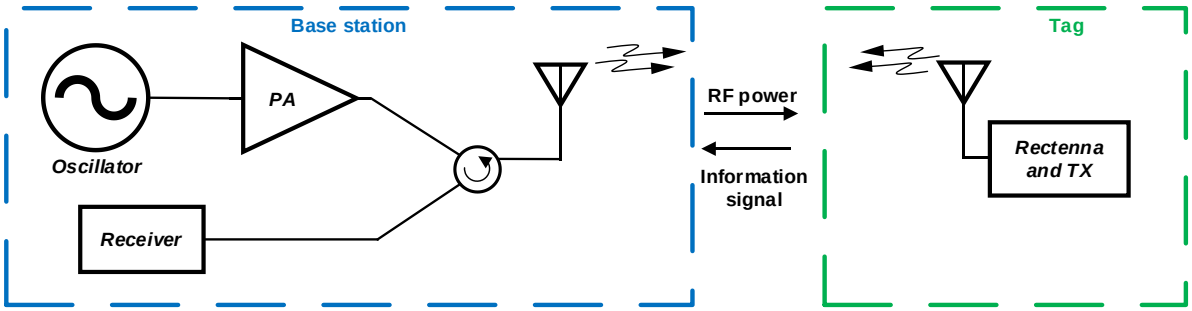

Figure 2-6: Block diagram of a SWIPT system.

2.3.1 Base station Architecture

As shown in figure 2-7 the base station transmitter consists of an oscillator and an amplifier. The schematic for these components is shown in figure 2-7, with the input matching network (IMN) intended to maximize power transfer from the oscillator to the amplifier. In the schematic C1, C2 and C3 are used as DC blocks while L4 and L5 are used as RF chokes and DC feeds. As inductors can be difficult to implement at frequencies greater than 1 GHz, these inductors can be substituted for quarter wavelength transmission lines. Resistor R1 and R2 block RF from the DC biasing and limit the current for the high electron mobility transistors (HEMT) M1 and M2. Components C1, L1, C2, L2, and L3 construct the feedback network for the oscillator. The complete design and optimization for this structure is explained in chapter 5.

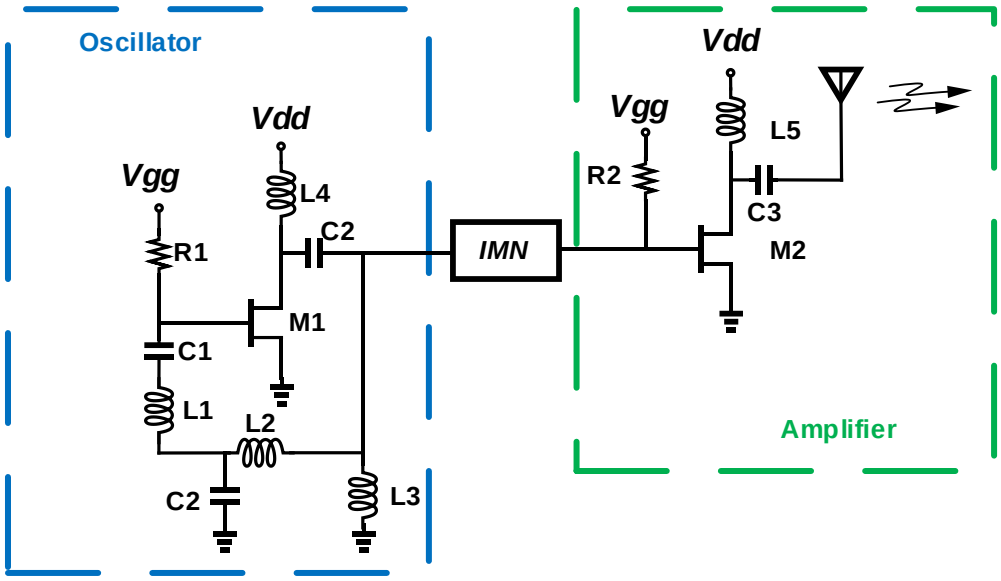

Figure 2-7: Base station transmitter.

2.3.2 Barkhausen Criteria

The general structure of a feedback oscillator is shown in figure 2-8. The transfer function can be described using the equation (8) below.

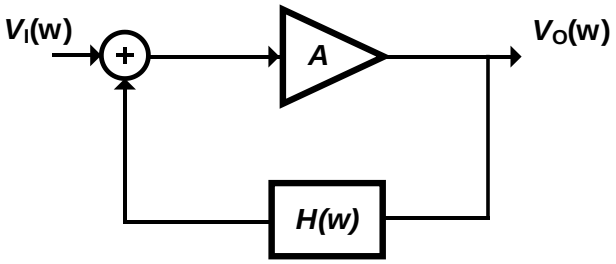

Figure 2-8: Oscillator generation structure.

$$TF(\omega) = \frac{V_o(\omega)}{V_I(\omega)} = \frac{A}{1 - AH(\omega)} \tag{8}$$

An oscillator is designed so that the denominator is equal to zero at a particular frequency [17]. This condition is known as the Barkhausen criteria and can be summarized from equations (9) and (10) below. The lumped components in the feedback network for the circuit shown in figure 2-7 are used to achieve the required loop gain and phase for stable oscillation.

$$Loop\ Gain|AH(\omega)| = 1 \tag{9}$$

$$\angle AH(\omega) = 0 \tag{10}$$

In additional to following the Barkhausen criteria, there must be a startup condition to achieve stable oscillation [16]. The transients in the power supply or thermal noise from the components is often sufficient to meet this start up condition.

2.3.3 Phase Noise and Figure of Merit

Phase noise represents the fluctuations in the frequency of an oscillator signal and is a vital metric in oscillator design. Figure 2-9 compares an ideal power spectrum density (PSD) of an oscillator to one that exhibits phase noise. The non-ideal oscillator produces an output over a range of frequencies while the ideal one produces a signal tone. The multiple frequency components evident in the non-ideal PSD are in part a result of the feedback network, $H(w)$, having a non-zero bandwidth [16]. This results in the loop gain being nonzero for a range of frequencies, enabling the output waveform to contain multiple frequency components.

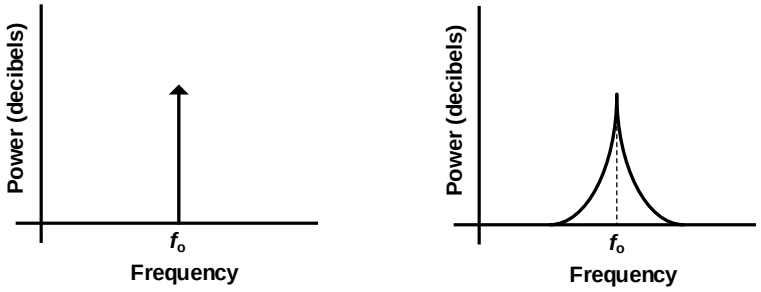

Figure 2-9: PSD of an ideal oscillator compared to realistic.

The units for phase noise are dBc/Hz and it is measured relative to the carrier signal. At a given offset frequency $\Delta\omega$ phase noise of an oscillator can be expressed as [22]

$$L(\Delta\omega) = 10\log\left(\frac{\sum F}{P_{RF}}\left(\frac{\omega_o}{\Delta\omega}\right)^2\right) \tag{11}$$

In this equation $\sum F$ is a function of the total effective noise generated by the circuit elements, ω_o is the oscillator frequency and P_{RF} is the output RF power.

An oscillator figure of merit (FoM) summarizes its performance and allows for straightforward comparison between different designs. FoM is calculated using equation (12) below, where $L(\Delta\omega)$ is the phase noise for at a given frequency offset, $\Delta\omega$, from the fundamental frequency, ω_O, and $P_{DC,mW}$ is the DC power consumption in milliwatts [23].

$$FoM = 10\log(L(\Delta\omega) * \left(\frac{\omega_o}{\Delta\omega}\right)^2 P_{DC,mW}) \tag{12}$$

2.3.4 Low Power Communication Methods for Tag

While a WPT oscillator can be powered off conventional energy sources, the tag must be self-sufficient and rely on the energy received by the antenna. This makes the generation of RF signals at the tag very challenging since very little power is available. To address this issue, communication methods have been developed that convey information by reflecting or absorbing the received signal or use the nonlinearities generated by a rectenna as a carrier signal.

RF backscattering is the process in which information is conveyed by reflecting or absorbing the incident RF signal [24] [25]. Backscattering is already featured in numerous commercial and industrial applications, one of the most common examples is RFID. Figure 2-10 shows a conventional backscattering system. It consists of an antenna, a switch, and various loads.

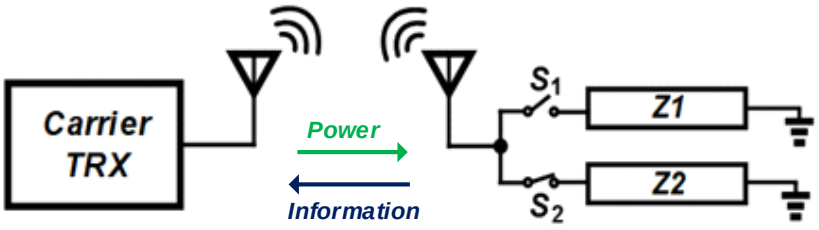

Figure 2-10: Conventional backscattering systyem.

The carrier TRX transmits a signal and the tag switches between two impedance states. A load impedance match to the antennas impedance results in an absorbed signal, while a load impedance much smaller than or larger than the antennas impedance, results in a complete reflection ($\Gamma_s = 1$) of the incident signal. The reflected signal can then be received by the carrier emitter or another tag. A '1' bit corresponds to a receiving a signal while no received signal conveys a '0' bit. The

reflection and absorption can be explained by equation (13) where Z_s represents the antenna impedance and Z_o represents the impedance state.

$$\Gamma_s = \frac{Z_s - Z_o}{Z_s + Z_o} \tag{13}$$

The carrier TRX in many applications is a dedicated transmitter that supplies power and a carrier signal to the tag. Recent research however has worked to remove the dedicated transmitter and uses ambient RF signals as a carrier signal [24-29]. These systems are called ambient backscattering communication systems (ABCs) and do not require dedicated frequency spectrum, which is scarce and expensive [24]. ABCs devices can also combine to form large sensor networks and will be a major component in future IoT applications [24].

While backscattering has shown its merits in low power communications, it has limited applicability due to self-jamming when used in full duplex communication where information is being transmitted and received at the same time [30]. Figure 2-11 demonstrates this concept for a bistatic backscattering architecture, a communications structure where the transmitter and receiver are separated and do not share the same antenna [24]. The WPT transmitter supplies RF energy to the tag which modulates the signal and backscatters it to a receiver. However, the signal emitted by the WPT transmitter is also received by the receiver. This undesired signal is often received at a much stronger power level than the tag's signal and as a result, the information transmitted from the tag is often indecipherable.

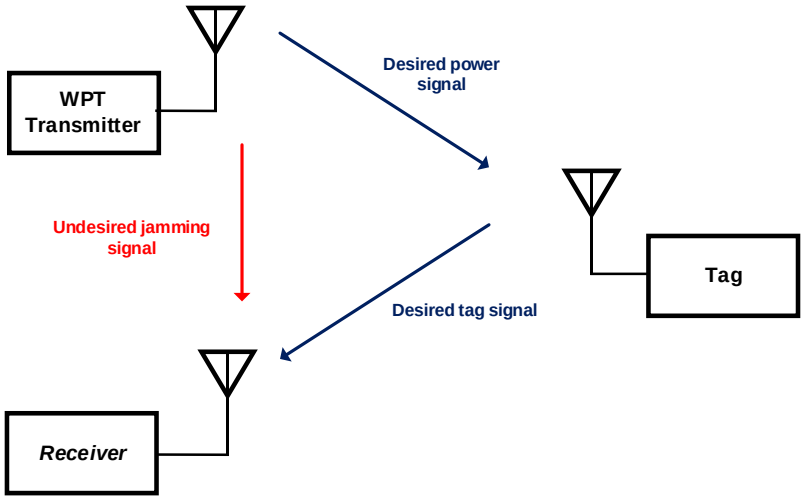

Figure 2-11: Self jamming in a bistatic architecture.

The self-jamming issue is mitigated by using a monostatic architecture, a communication structure where the transmitter and receiver are collocated and use the same antenna. A circulator is used to isolate the received signals from the transmit signals, however there is still an interference issue as the ports are not fully isolated from each other [30] [31]. This issue is illustrated in figure 2-12. A monostatic structure is useful when the tag is close to the transmitter, as the low propagation loss allows for the received signal to be stronger than the interfering signal from the TX leakage. The range can be expanded using self-interference cancellation methods, but these often add a great amount of complexity to the system [30] [31].

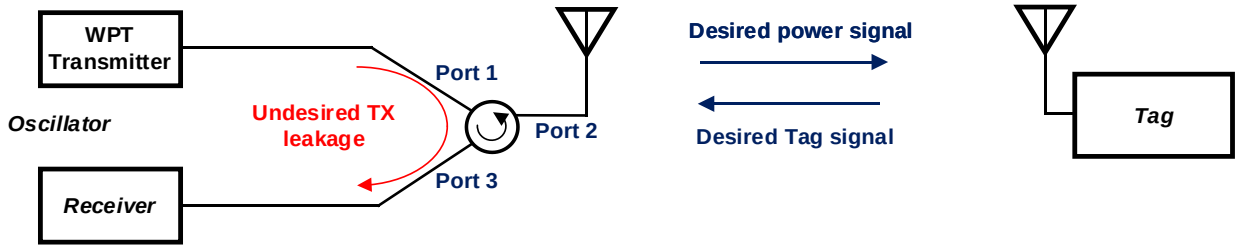

Figure 2-12: Self jamming in a monostatic architecture.

One of the most effective and simplest methods to mitigate the self-jamming issue is by separating the transmit and receive frequencies, known as frequency duplexing. This allows for the undesired signal from a collocated or separate transmitter to be filtered out. The tag can synthesize a carrier signal at a separate frequency by utilizing the harmonics generated by the

rectennas rectifier. This avoids the use of power hungry, conventional, frequency synthesis methods. The ability of a rectifier, such as the voltage doubler shown in figure 2-3, to synthesize a carrier signal can be explained using a mathematical model for a nonlinear memoryless system. [17] [32 – 34]

$$y(t) = \alpha_0 + \alpha_1 x(t) + \alpha_2 x^2(t) + \alpha_3 x^3(t) \tag{14}$$

Here $y(t)$ represents the output, $x(t)$ represents the input, and the α terms represent Taylor expansion coefficients. For a sinusoidal input of

$$x(t) = A\cos(2\pi f t) \tag{15}$$

The first four terms of the output can be expressed as

$$y(t) = \alpha_0 + \alpha_1 A\cos(2\pi f t) + \alpha_2 A^2 \cos^2(2\pi f t) + \alpha_3 A^3 \cos(2\pi f t)^3 \tag{16}$$

Using trigonometric identities this can be expressed as

$$y(t) = \alpha_0 + \frac{\alpha_2 A^2}{2} + \left(\alpha_1 A + \frac{3\alpha_3}{4} A^3\right)\cos(2\pi f t) + \frac{\alpha_2 A^2}{2}\cos(4\pi f t) + \frac{\alpha_3 A^3}{4}\cos(6\pi f t) \tag{17}$$

The DC terms, the terms with no frequency component, are used for energy harvesting while the harmonics generated, that are multiples of the input frequency, can be used as a carrier signal. The spectrum of a typical rectifier output for a single tone input is shown in figure 2-13, while a small portion of the input frequency f_1 bleeds through, the second and third harmonics are typically the highest produced tones. Figure 2-14 shows a block diagram of a tag that can synthesize its own signal. The DC and harmonic frequency can be separated at the output using a low and high pass filter. The harmonic signal is then modulated to convey information and transmitted to a receiver. The DC load can be a sensor or microcontroller.

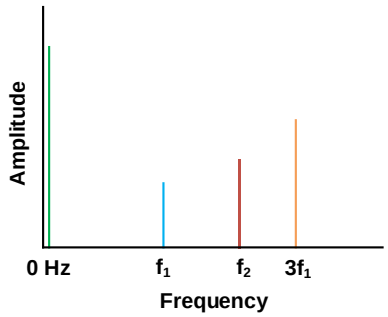

Figure 2-13: Spectrum of rectifier.

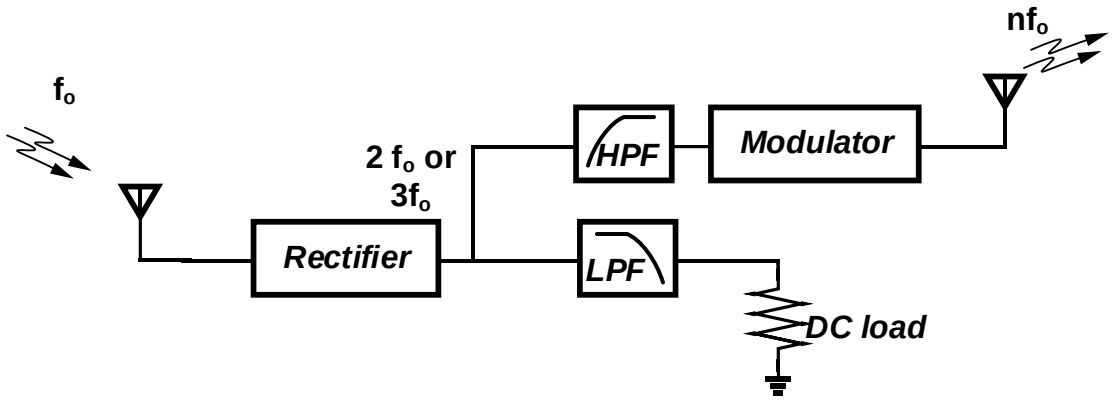

Figure 2-14: Block diagram of harmonic feedback tag.

Both backscattering and utilizing the harmonics generated by a rectifier are useful low power communication methods. While frequency duplexing can improve the signal to noise ratio at a receiver, the harmonic signals generated are only a fraction of the received signal power and have limited transmission range. Backscattering, on the other hand, does not require any frequency conversion and can transmit a higher power signal towards the receiver. The concepts of backscattering and harmonic extraction will be further investigated in chapters 4 and 5.

2.4 Chapter Summary

This chapter explains the key concepts for understanding simultaneous wireless information and power systems. Ambient RF energy sources are discussed along with the design of dedicated WPT transmitters. Two low power communication schemes that can be utilized by wireless sensor nodes for IoT applications are also examined.

Chapter 3: Design of an Efficient 2.4 GHz RF Energy Harvester

This chapter presents the design and measurement valuation of a RF energy harvesting system developed to extract energy in the crowded 2.4 GHz ISM band. The developed rectenna uses multiple patch antennas and a differential rectifier topology to eliminate the power splitter at the input and achieve an RF-to-DC power conversion efficiency of 69.3% with 5.1 mW being delivered to the load. The system was simulated using Keysight ADS and the developed prototype was implemented on a Rogers 4003C substrate ($\epsilon_r = 3.55$). Section 3.1 provides a brief literature review of RF EH in the 2.4 GHz band. Section 3.2 describes the antenna, impedance matching, and rectifier design. Section 3.3 explains the simulation results and then Section 3.4 presents the developed prototype and measurement results. The chapter is concluded in section 3.5.

3.1 Literature Review

Various publications have investigated and developed rectenna designs to function in the 2.4 GHz band. Andia Vera et al. developed a compact rectenna system based on a dual polarized antenna [35]. The rectifier consists of a four-stage voltage multiplier and achieves the RF-to-DC PCE of a 42.1% for an input power of -10 dBm. The rectifier offers satisfactory efficiency at low input power, but the small output power for a low input power level is insufficient to drive the load for many applications. Olgun et al. proposed a differential rectifier that can achieve peak conversion efficiency of 68% given -5 dBm RF input power [36]. The power splitter at the input distributes power between two rectifier branches and adds loss. In another approach researchers demonstrated a RF EH system with a 58% conversion efficiency at 6 dBm input power [37]. While the design does not achieve as high PCE as other works, it utilizes a Wilkson power divider to harvest power from multiple patch antennas [37]. Multiple antennas enable it to harvest a significant amount of energy. Tafekirt et al. implemented three single-ended rectifiers in parallel [38]. Each rectifier matches to a specific frequency and the DC output voltages of three rectifiers are combined at the output. Although collecting power from different input RF signals with different frequencies increases the overall DC output voltage, the power splitter at the input degrades the PCE. The power splitter causes ohmic loss and leakage of the input power to undesired rectifier branches.

To address the issues in the abovementioned works, this paper proposes a differential RF energy harvester structure. The RF EH developed in this paper utilizes a modified Greinacher

rectifier topology to achieve RF-to-DC conversion efficiency of 69.3 % at the input power of 5.2 dBm at 2.4 GHz by removing the power splitter and combiner.

3.2 Design Methodology

As shown in literature, it is often desirable to use multiple antennas to enhance the energy received in a particular direction [36, 37]. Traditionally a power divider is used to connect the antenna elements, however this adds additional loss. To address this issue, a rectenna structure that eliminates the power splitter by using a differential topology is purposed. Figures 3.1 and 3.2 illustrate the traditional and developed rectenna systems, respectively.

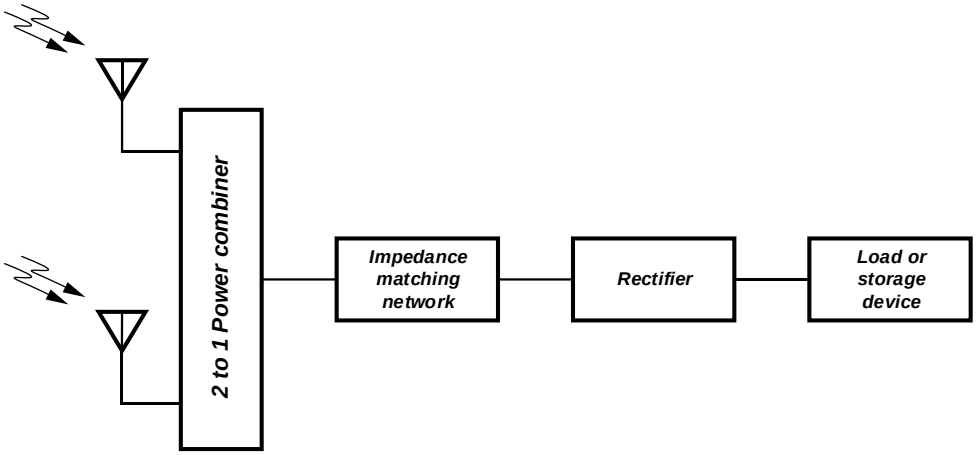

Figure 3-1: Conventional rectenna structure.

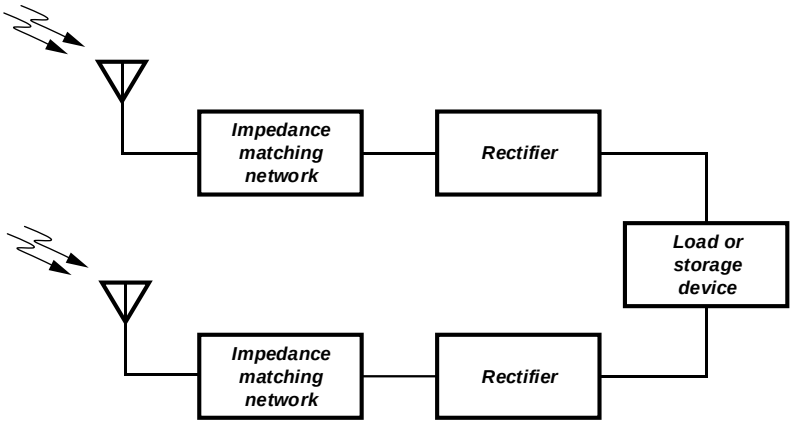

Figure 3-2: Proposed rectenna structure.

3.2.1 Antenna Design

Due to its moderate directivity and ease to implement on a printed circuit board the patch antenna is selected for the energy harvester. The basic structure of a patch antenna is shown in figure 3-3.

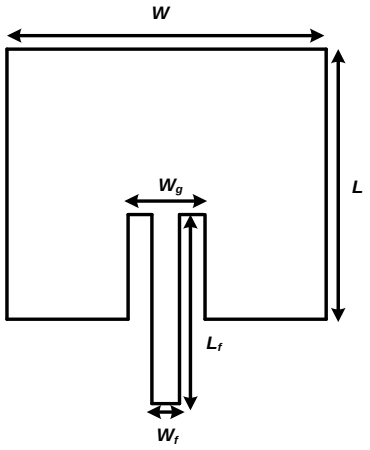

Figure 3-3: Patch antenna structure.

The steps used to determine its dimensions are presented below and follow the process discussed in [39] [40]. First, the width of the radiating patch element is calculated.

$$W = \frac{c}{2f_o\sqrt{\frac{\epsilon_r + 1}{2}}} \tag{18}$$

Here ϵ_r is the relative permittivity of the substrate ($\epsilon_r = 3.55$ for Rogers 4003C). f_o is the center resonant frequency, and c is the speed of light. The effective dielectric constant, which accounts for the height of the substrate h, is then found.

$$\epsilon_{reff} = \frac{\epsilon_r + 1}{2} + \frac{\epsilon_r - 1}{2}\sqrt{(1 + 12\frac{h}{w})} \tag{19}$$

The effective dielectric constant is used to calculate the effective length, L_{eff}, of the patch antenna.

$$L_{eff} = \frac{c}{2f_o\sqrt{\epsilon_{reff}}} \tag{20}$$

The effective length is larger than the actual length of the patch due to fringing effects. The actual length can be determined from the expression below.

$$L = L_{eff} - 2\Delta L \tag{21}$$

Where ΔL is equivalent to

$$\Delta L = 0.412h\frac{(\epsilon_{reff} + 0.3)(\frac{W}{h} + 0.264)}{(\epsilon_{reff} - 0.258)(\frac{W}{h} + 0.8)} \tag{22}$$

The inlet feed was used to match the antenna to 50 ohms. The calculated values and inlet feed size were adjusted to optimize the gain and return loss of the antenna. Table 3-1 compares the calculated values to the optimized values.

Table 3-1

Parameter	Calculated Value (mm)	Optimized Value (mm)
W	40.5	36
L	32.02	32
W_g	-	.8
W_f	-	2.2
L_f	-	17.8

The antenna was simulated using Keysight ADS and the gain was found to be 5.9 dBi. The simulated return loss was found to be $S_{11} < -30\ dB$ at 2.45 GHz.

3.2.2 Impedance matching network design

To allow for maximum power transfer, the rectifier input impedance must be equal to the conjugate of the source impedance, Z_s. The impedance of the rectifier can vary depending on the power level, frequency, and load resistance [41]. To account for the nonlinear operation of the rectifier, the source pull (SP) method was used to design the input matching network. Figure 3-4 shows the schematic diagram for SP simulations. The source impedance is swept, and the efficiency, $\eta = \frac{V_{out}^2}{P_{RF} R_L}$, is plotted for each impedance value.

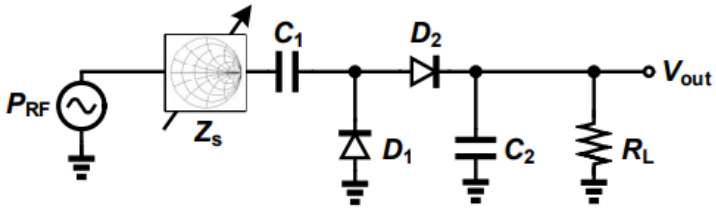

Figure 3-4: Test set up for source pull simulations.

Figure 3-5 shows the simulation results for an input power of 10 dBm and an output load of 11 kΩ. If source impedance is the innermost contour of (7.5 + j29) Ω, the rectifier achieves the maximum RF-to-DC efficiency of 74%. The efficiency gradually decreases as the contours move further away from the inner most one. The simulation results show that the input impedance of the rectifier circuit is (7.5 – j29) Ω. The proposed rectenna adopts an open circuit T- branch structure for the matching, and Figure 3-6 shows the proposed structure with dimensions in millimeters, along with the rest of the rectifier.

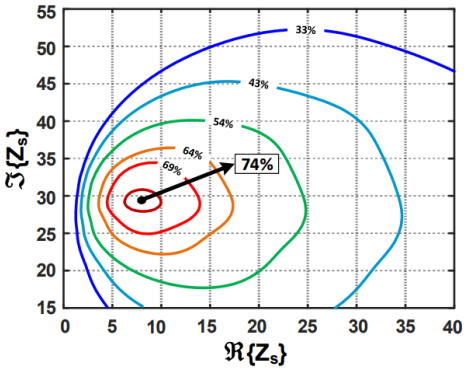

Figure 3-5: Simulated source pull contours.

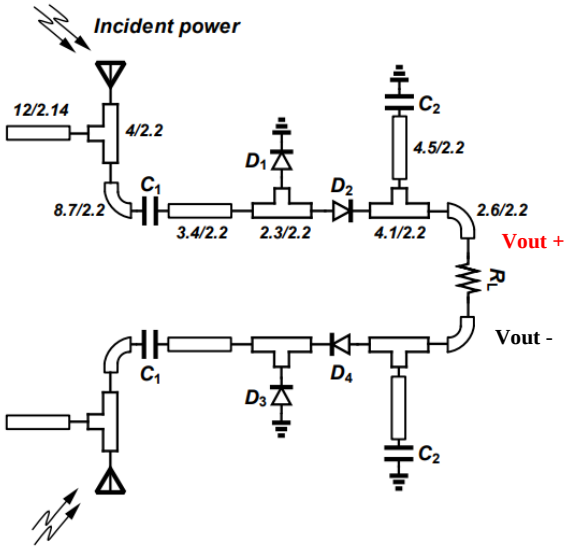

Figure 3-6: Proposed rectenna with impedance matching strucutre.

3.2.3 Rectifier Design

The differential rectifier topology shown in figure 3-6 is selected for the rectenna as it allows for the removal of a power splitter or DC combiner. Each side is composed of two voltage doublers and connected to a common load. The V_{out}^{+} terminal of the rectifier should have approximately 2 time the input voltage, while the V_{out}^{-} terminal should have -2 times the input voltage. The V_{out}^{+} and V_{out}^{-} voltages are combined at the output through the load resistance R_L.

The Skyworks 7630 Schottky diodes are used for the proposed rectifier [42]. These diodes offer a low threshold voltage and series resistance and have the specifications listed in

Table 3-2. We observed that these diodes are more efficient than similar low threshold diodes often used in RF energy harvesting.

Table 3-2: Spice parameters for Skyworks 7630 diode.

Parameter	Value
Saturation current	5 μA
Ohmic resistance	20 Ω
Transient time	10 psec
Zero bias junction capacitance	0.14pF
Junction potential	0.34 V

3.3 Simulation Results

The proposed rectenna and the patch antenna were laid out and simulated using Keysight ADS. The complete layout and radiation pattern of the antennas is shown in Figure 3-7. Figure 3-8 shows PCE and output voltage ($V_{out}^{+} - V_{out}^{-}$) for a given input power with a load of 11 kΩ. This load was found to provide the highest RF-to-DC PCE, 72.8%, for the given input power range. The RF-to-DC PCE efficiency was determined using equation 23 where $P_{RF_{total}}$ represents the total RF power at the input, and P_{RF} represents the power at the input of one voltage doubler.

$$\eta_{RF\ to\ DC\ PCE} = \frac{P_{DC}}{P_{RF_{total}}} = \frac{(V_{out}^{+} - V_{out}^{-})^2}{2P_{RF}\,R_L} \tag{23}$$

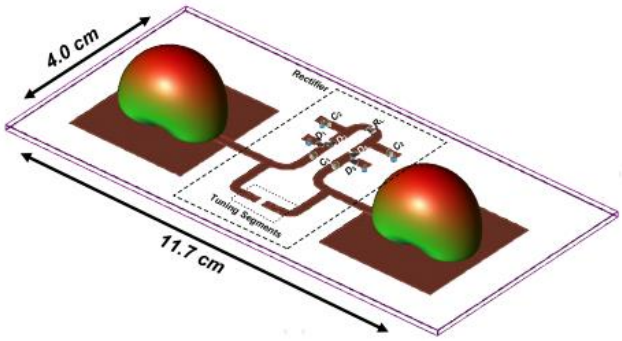

Figure 3-7: Layout of proposed rectenna.

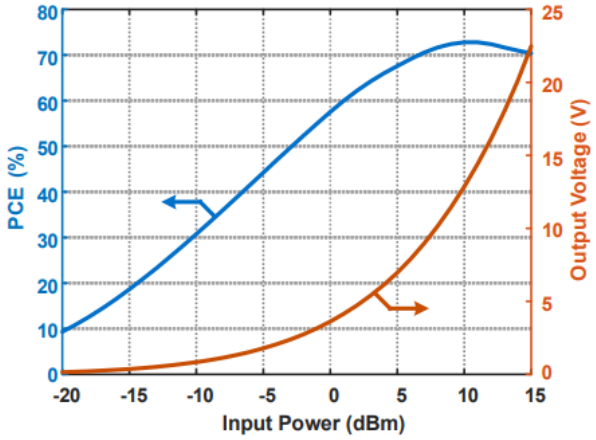

Figure 3-8: Rectenna PCE and output voltage over input power range at 2.45 GHz.

The proposed rectifier exhibits a high sensitivity as it is capable of harvesting energy at input power levels below -20 dBm. The rectenna matching network could be redesigned to operate obtain a higher PCE at lower input power levels. However, this results in a lower overall PCE especially at higher input powers. Figure 3-9 shows that PCE is a function of the input power and load resistance.

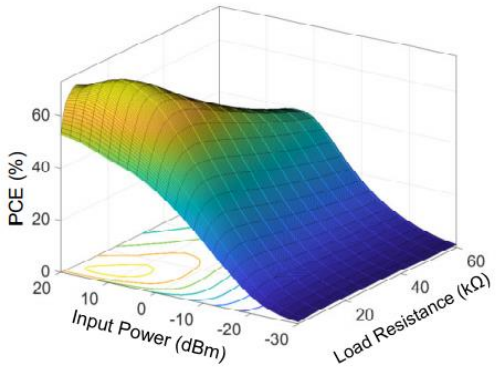

Figure 3-9: Rectifier PCE versus input power and load resistance at 2.45 GHz.

3.4 Measurement Results

The proposed rectenna was prototyped on Rogers 4003C substrate. This material was selected because it offers a low variation in permittivity and low loss at high frequencies compared to other common PCB substrates, such as FR-4 [43]. The size of the complete rectenna is 4.0 cm × 11.7 cm, and its thickness is 1.6 mm. The S-parameters of the rectifier and antenna were measured using the R&S ZVA 67 vector network analyzers and the results are shown in figure 3-10 and figure 3-11, respectively. A frequency shift is present between the simulation and experiment results for antenna S_{11} parameter. While the antenna was designed for 2.45 GHz, it matches to 2.4 GHz due to process variations in manufacturing. This range is acceptable as the 2.4 GHz band still encompasses a large amount of ambient RF energy, ex. WiFi (IEEE 802.11).

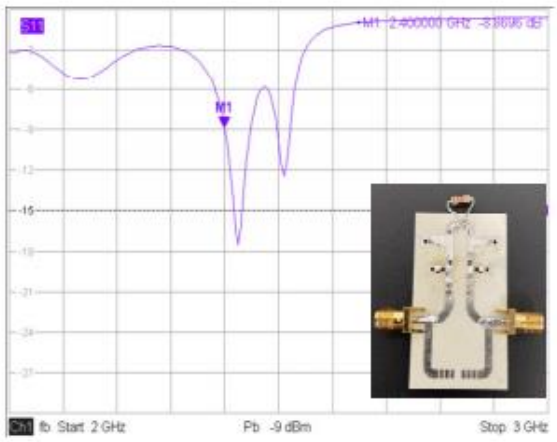

Figure 3-10: Measure S_{11} for rectifier.

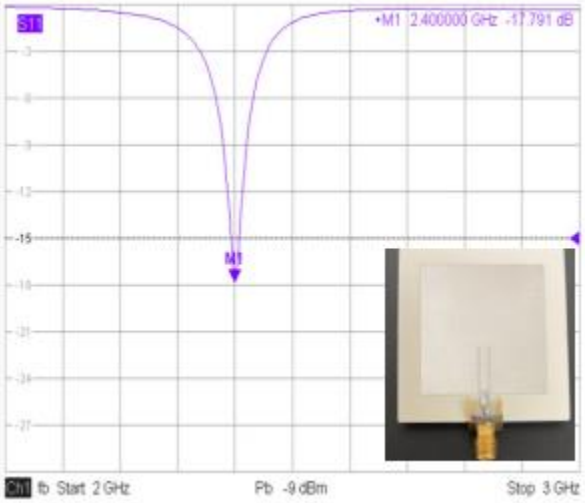

Figure 3-11: Measured S_{11} for antenna.

Figure 3-12 shows the experimental setup to measure RF-to-DC PCE. An Agilent EE438C ESG vector signal generator, tuned to 2.4 GHz and connected to a patch antenna identical to the ones used on the rectenna, is used as a transmitter. The transmitting antenna was placed 10 cm away from the rectenna. The Friis formula for free space loss (equation 6) is used to calculate the received power at the patch antennas of the rectenna, in which the gain of the transmitting and receiving antennas are 5.9 dBi. The effective path loss between the transmitter and the receiver as well as loss in cables is calculated as 9.33 dB.

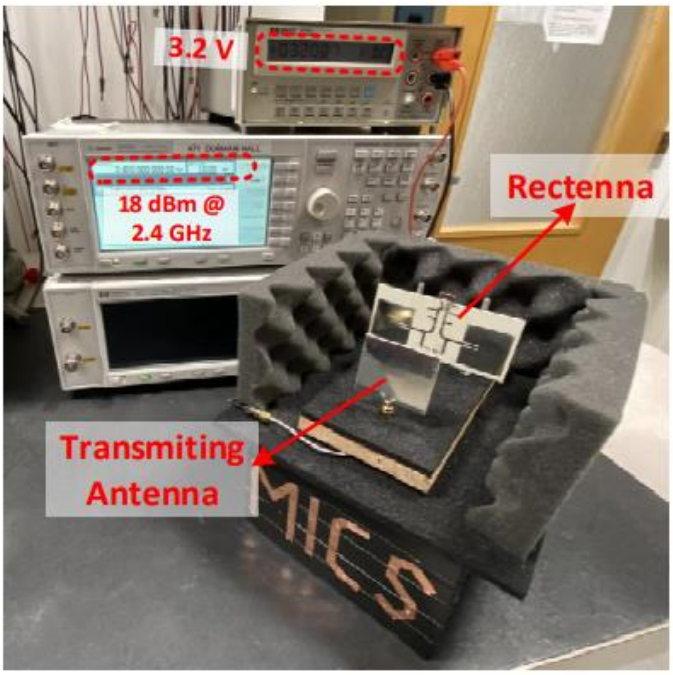

Figure 3-12: Measurement setup for rectenna.

Figure 3-13 shows the PCE and the output voltage of the proposed rectenna for a 2.4 GHz signal. The PCE increases steadily as the received power increases and then decreases rapidly after reaching the peak point. The peak PCE is 69.3 %; this is achieved when the received power is 5.2 dBm for a single antenna or 8.2 dBm for two antennas of the rectenna. The transmitter power is 18 dBm at the peak PCE point and the output power delivered to the load resistor is 5.1 mW. The measured peak PCE is lower than the simulated one by 3.5 %, which is reasonable considering process variations. The output voltage across the load resistor increases steadily with increase of the received power and saturates to nearly 3.5 V after the received power of 7 dBm.

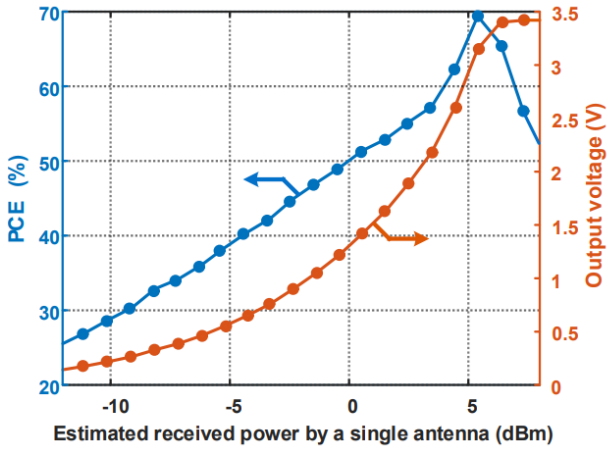

Figure 3-13: Rectenna PCE and output voltage for given transmitted power.

Table 3-3 compares the proposed rectenna with other RF energy harvesters. The proposed rectenna achieves the highest PCE compared to previous works. In addition, the proposed rectenna achieves highest dc output power with the input power ranging from 0 dBm to 8 dBm. This can be attributed to the removal of the lossy power divider and the using two antennas to harvest received RF power.

Table 3-3 Comparison between prior RF EH works

Specification	[35]	[36]	[37]	[38]	This work
Frequency (GHz)	2.45 GHz	2.45 GHz	2.42	2.45	2.4 GHz
Diode	SMS 7630	HSMS 2852	HSMS 285B	HSMS 2852	SMS 7630
Substrate	Arlon A25N	RO3206	RO3206	FR4	RO4003C
Peak PCE	4 5%	68 %	58 %	47.5 %	69.3 %
P_{in} at peak PCE	0 dBm	-5 dBm	8 dBm	3 dBm	5.5 dBm
DC output power	0.48 mW	0.60 mW	0.60 mW	0.48 mW	1.0 mW

3.5 Chapter Summary

This paper presents a 2.4 GHz rectenna for RF energy harvesting. The rectifier adopts a differential topology to eliminate the power splitter at the input and the voltage adder at the output. The source pull matching technique is used to match the input impedance of the rectifier to the 50

Ω patch antenna. The rectenna is prototyped with Rogers 4003C substrate. The measurement results indicate that the rectenna achieves the peak power conversion efficiency of 69.3 % at the frequency of 2.4 GHz. The high efficiency is due to removal of the power splitter and by using the low-loss Skyworks 7630 diode.

Chapter 4: Efficient Backscatter Modulation for IoT Applications

This chapter presents a compact backscatter modulator tag operating at 1.76 GHz. The modulator is composed of a series combination of a variable resistor and a varactor. These components modulate the backscatter signal by adjusting the input impedance or input reflection coefficient. A gallium nitride (GaN) on silicon carbide (SiC) high electron mobility transistor (HEMT) is adopted to implement the variable resistor. The modulator can support a variety of modulation schemes without increasing the size and design complexity. The tag can be continuously powered through ambient RF energy in the 2.45 GHz frequency band. A differential rectifier, similar to the one designed in chapter 3, harvests RF energy to power a microcontroller eliminating the need for a battery. Experimental results show that the modulator can support 16-QAM with an error vector magnitude (EVM) of 1.73%. The measured RF-to-DC power conversion efficiency (PCE) of the energy harvester is 57.1% at a received power of 1.7 dBm. Section 4.1 discusses prior works related to RF backscattering. Section 4.2 describes the methodology followed to design the modulator and energy harvester. The developed circuit is then experimentally validated in section 4.3 and the chapter is concluded in section 4.4.

4.1 Literature Review

As discussed in section 2.3, backscattering RF signals can greatly reduce the power consumption of wireless sensor nodes. There are numerous prior works that propose backscatter communication systems. Daskalakis et al. [44] developed an ambient FM backscattering system for agricultural applications. The system consists of a low power microcontroller, which toggles switches with different load impedances. A super capacitor charged through RF energy harvesting provides the power for the backscattering system. The device featured a low design complexity, but the simple ON-OFF modulation limits its data rate and is spectrally inefficient. Thomas et al. [45] developed a high bit rate, 16-QAM backscatter by utilizing four sets of single pole four throw (SP4T) switches. The drawbacks of the design are that switches take up a significant amount of space and are difficult to power solely through ambient RF energy. In another work, Daskalakis et al. [46] developed a low powered ambient backscattering transmitter that utilized 4 – PAM. The transmitter adopts an active load as the modulator, which is realized by a single RF transistor driven by a digital-to-analog converter (DAC). Four distinct impedance levels are achieved by

modulating the gate voltage of the transistor. It would be challenging to employ higher order modulation because of transistors limited variation in the parasitic capacitances. Correia et al. also utilized transistors to develop a backscatter modulator [47]. The design adopts a dual band Wilkinson power divider to generate a 4-QAM modulation using ambient 900MHz and 2.45 GHz signals. By backscattering multiple frequencies, they achieved a high bit rate of 500kps. However multiple transmission frequencies complicate the receiver design.

To address these shortcomings, this paper proposes a backscatter tag capable of high order QAM modulations. The device is capable of being powered by ambient RF energy and backscatters signals in the ambient GSM 1.8 GHz band. The tag utilizes a HEMT operating in the triode region, as well as a commercial-off-the-shelf (COTS) varactor to emulate district impedances. The varactor and transistor can be controlled by a low power microcontroller, which can be powered by the energy harvested by a 2.45 GHz rectifier like the one developed in chapter 2.

4.2 Design Methodology

4.2.1 Backscatter Tag Design

Backscatter QAM modulation is achieved by carefully adjusting the load impedance presented to a receiving antenna. A N-QAM I-Q constellation requires N number of load impedances [45] [23], where each symbol on the constellation is expressed in equation 24.

$$S_i = x_I + jy_Q \tag{24}$$

where x_I represents the in-phase component and y_Q represents the quadrature component for a given symbol, S_i. For the passive backscattering case, each symbol must be scaled to fit on the Smith chart [48]. This can be achieved by using the expression shown in equation 25.

$$\Gamma_L = \alpha \frac{S_i}{\max|S_i|} \tag{25}$$

where α ranges from 0 to 1 and represents the scaling factor and Γ_i is the reflection for a given constellation point [49]. As α moves closer to 0, the constellation points move closer together on the Smith chart. This simplifies the circuit design as fewer components are needed and lower biasing ranges can be used. Having said this, large α values are desirable as spread apart

constellation points provide higher reflected powers to the intended receiver, increasing SNR [49]. It can be complicated to design a circuit that exhibits a large scaling factor with minimal complexity and biasing conditions.

The circuit presented in this paper achieves a scaling factor of 0.45. Figure 4-1 shows the constellation diagram for 4, 16, and 64 QAM. The constellations are shifted to the right due to the channel resistance and capacitance range of the GaN HEMT and the varactor. This range also determines the scaling factor. The load impedances required to generate each constellation state is calculated from equation 26.

$$Z_L = \frac{Z_0(1+\Gamma_L)}{1-\Gamma_L} \tag{26}$$

where Z_0 and Z_L represent the source impedance and load impedances, respectively. The source impedance is typically a 50 Ω antenna. Table 4-1 lists the required load impedances to cover the four-reflection coefficient at the corners of the constellation. These values correspond to the maximum and minimum values of the resistance and reactance. The impedance values in Table 4-1 are realized using a zero-biased Cree CGH40006P RF GaN HEMT as a variable resistor and the Skyworks 1248 varactor for its variable reactance [50]-[51].

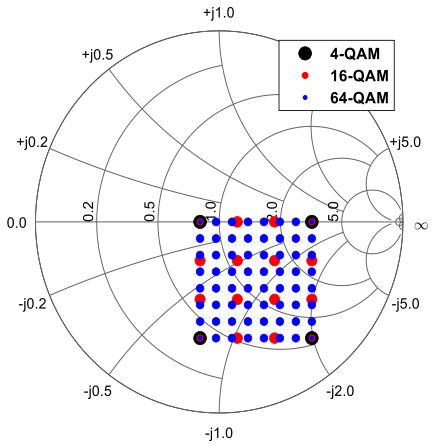

Figure 4-1: Ideal 4,16, and 64 QAM constellation.

Table 4-1 Corner reflection and impedance values for a 16 – QAM constellation.

#	Γ_L	Z_L
1	0.104 ∠ 180°	40.6 ∠0.925°
2	0.609 ∠ -99.7°	42.9 ∠ -62.3°
3	0.504 ∠ 0°	151 ∠1 .24°
4	0.783 ∠ -50.3°	104 ∠ -72.2°

4.2.2 Backscatter Tag Component Modelling

A simplified, equivalent model for the GaN HEMT is shown in Figure 4-2. The model is developed based on the Angelov model in triode region [52]. R_{eq} is the series combination of the parasitic resistances in the drain, source, and intrinsic channel of the transistor. L_D, L_S and C_{pd} are the parasitic inductances at the drain and the source and the pad capacitance, respectively. Figure 4-3 (a) shows the resistive and reactive terms of the drain impedance for the selected GaN HEMT at 1.8 GHz. The real part is taken as the variable resistance and controlled through the gate bias voltage and the reactive part is absorbed to form the imaginary term in (1). As the gate bias voltages increase from -3V to -2V, the channel resistance ranges from 53 Ω to 8.9 Ω. The chosen GaN HEMT features a large range of resistances in the deep triode region with minimal changes in biasing in comparison to other RF transistors. This enables the modulator to support higher order modulation schemes while achieving relatively low error vector magnitude (EVM).

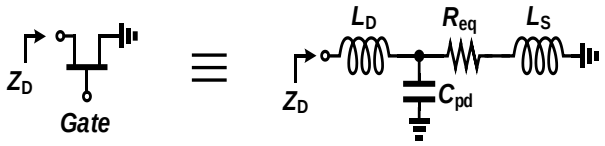

Figure 4-2: Simplified equivalent model of GaN HEMT in triode region.

Keysight ADS simulations were conducted to simulate the backscatter modulator. The GaN HEMT model was obtained from the manufacture and proven accurate in previous works [53]-[55]. The large signal model of the varactor diode, including the parasitics of the package, was also used. Figure 4-3 (b) shows the equivalent resistance and capacitance versus the control voltage applied across the varactor. As the applied reverse voltage increases from 0 to 5V, the capacitance of the varactor decreases from 22 pF to 1.49 pF, while its resistance decreases from 3.8 Ω to 1.8 Ω. When the transistor is operating near the cut off region ($V_{GS} \approx$ -3V) the varactor resistance is negligible. However, the resistance is significant in the deep triode region ($V_{GS} \geq$ -2.8 V).

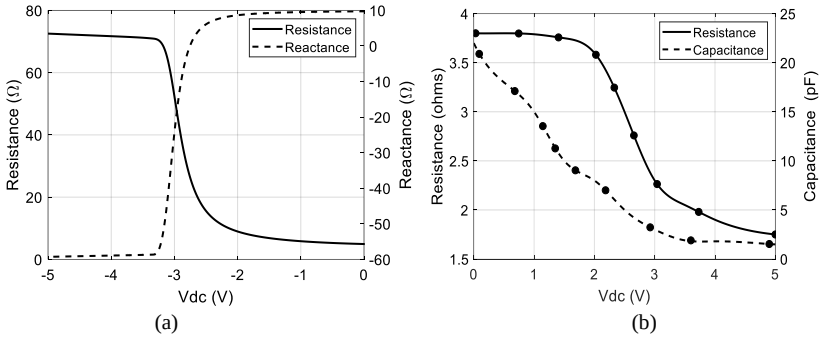

Figure 4-3: (a) Resistive and reactive portion of GaN HEMT drain impedance and (b) measured resistance and capacitance of varactor.

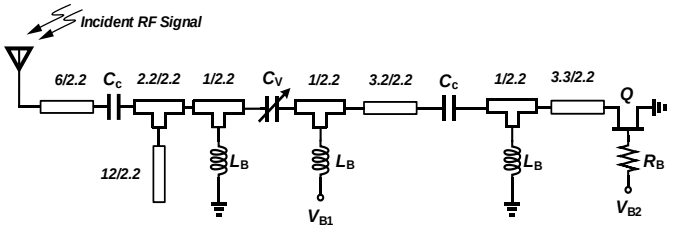

Figure 4-4: Schematic of proposed backscatter with the dimensions (length/width) in mm.

Figure 4-4 shows the schematic of the backscatter transmitter where capacitors labeled as C_c are ac-coupling capacitors and inductors labeled as L_B are RF-chokes. The microstrip L-section

at the input of the modulator is designed to shift Γ_L values to minimize the component biasing range, while achieving a sufficiently large range of impedance values.

4.2.3 Rectifier Design

To minimize the size, the rectifier proposed in Chapter 3 was redesigned to function with only one antenna. The selected rectifier topology, along with the dimensions of the transmission lines, is shown in figure 4-5. The topology utilizes the same differential structure, but the power divider is included, and a FR-4 substrate is used. Simulation results showed the loss of the power divider to be 0.3 dB.

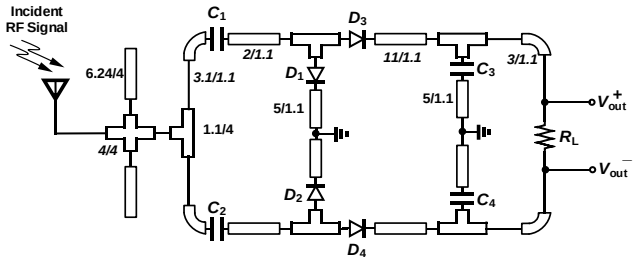

Figure 4-5: Schematic of proposed energy harvester with the dimensions (length/width) in mm.

Although a single antenna structure, power divider, and lossy FR-4 substrate will result in lower PCE and harvestable RF power, this rectifier structure is selected as it can feature minimal size and still fulfill the power requirement. Simulation results the rectifier can achieve a sufficient PCE at a 1 dBm input which is sufficient to power an 8-bit microcontroller such as the PIC 15LF1454 [56]. The FR-4 substrate also offers a higher permittivity which decreases the wavelength size for a transmission line. While the rectifier structure proposed in chapter 3 is more versatile, the structure shown in figure 4-5 was found to be suitable for the backscatter modulator.

4.3 Measurement Results

The proposed energy harvester and backscatter modulator is assembled on a FR-4 (ε_r = 4.6) PCB substrate. The size of the complete system is 5.5 cm x 4.2 cm and has a thickness of 1.6 mm. The test setup to measure the impedance states for a 16-QAM constellation and the RF-to-DC conversion efficiency of the rectifier is shown in figure 4-6.

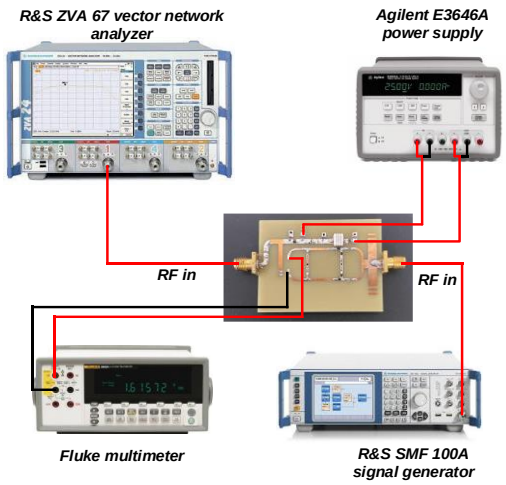

Figure 4-6: Measurement setup for rectifier and backscatter measurements.

The R&S SMF 100A signal generator is used to model the ambient 2.45 GHz energy. The output power is measured at various resistive loads to find the peak efficiency. Figure 4-7 shows the optimal rectifier measurement using a 4.5 kΩ load. The maximum RF-to-DC PCE was 57.1% at the input power of 1.7 dBm. At this condition, the output voltage and current were determined to be 1.95 V and 0.433 mA, respectively. These conditions are sufficient to power a microcontroller.

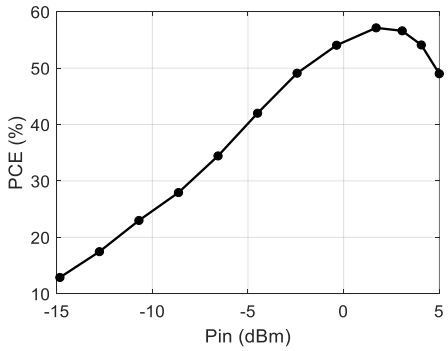

Figure 4-7: Measured energy harvester PCE over input power range.

The R&S ZVA 67 vector network analyzer was used to measure the impedance states for a 16-QAM constellation. The results are shown in Figure 4-8 and is a close match to the ideal constellations.

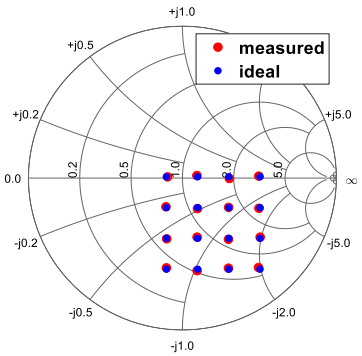

Figure 4-8: Measured 16-QAM impedance states versus ideal constellation.

The error vector magnitude (EVM) for a 16-QAM constellation is obtained as 1.73% using equation 27. Figure 4-9 shows the measured constellation on the IQ plane. There are minimal fluctuations in the impedance states for each measurement, and the EVM of the proposed backscatter is well below the 3.62% EVM for 16-QAM modulator found in [45].

$$EVM = \sqrt{\frac{\frac{1}{N}\sum_{k=1}^{N}\left|S_{K\,Ideal} - S_{K\,Measured}\right|^2}{\max S_{Ideal}}} \tag{27}$$

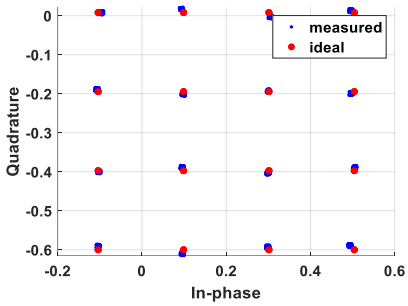

Figure 4-9: Measured 16-QAM constellation in IQ plane.

To achieve the constellation the HEMT gate biasing ranges varied from -4V to -1 V, and the reversed biased varactor voltage ranges from 0 to 5V range. The optimal backscattering frequency of 1.76 GHz was found as opposed to 1.8 GHz in simulations. This shift is reasonable and is a result of process variations.

A major advantage of using a varactor and GaN HEMT, as opposed to fixed impedance switches, is the constellation can easily be altered to model different modulation complexities. EVM can also be minimized as the impedance can be adjusted. Figure 4-10 shows a 64-QAM constellation

for the proposed backscatter. Unlike the circuit in [45], the proposed backscatter can implement a different QAM constellation by adjusting the gate bias and varactor voltage. However, as the case with all backscattering systems, the increase in modulation order results in each point on the constellation being closer together. This can deteriorate the bit error rate performance and complicates the receiver design.

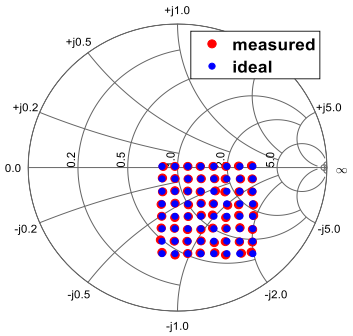

Figure 4-10: Measured 64-QAM IQ constellation versus ideal constellation.

Figure 4-11 shows a schematic diagram of the proposed backscatter with the bias voltage set up. A low power microcontroller with a DAC should be able to bias the varactor while the GaN HEMT can be biased using a DAC and a level shifter. To obtain the negative voltages required to bias the GaN HEMT the negative differential port of the energy harvester can provide a reference voltage for the level shifter.

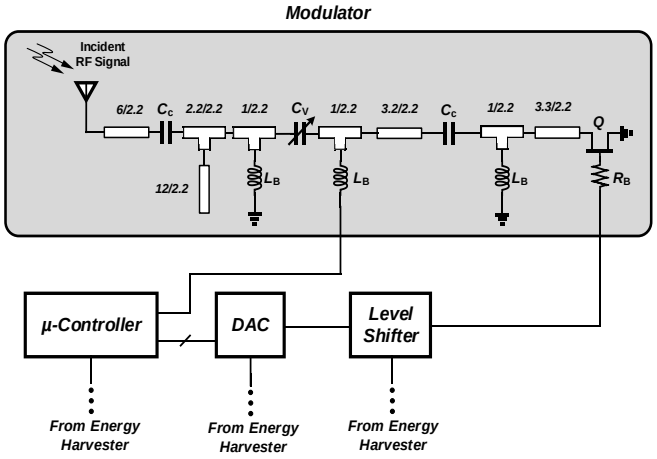

Figure 4-11: Complete biasing setup for the proposed backscatter tag.

Table 4-2 compares the proposed backscatter system to prior works. Unless noted otherwise, the energy/bit for each work was determined by dividing the power consumption of the modulator by

the bit rate. In this work the power consumption of the modulator was estimated by measuring the simulated DC power consumption in Keysight ADS. It was found that the GaN HEMT and varactor dissipated 2.06 uW at a symbol rate of 16 Mbps. From these results, it can be estimated that the modulator would exhibit and energy per bit rate of 21.4 fJ/bit using a 64 QAM modulation with a total bit rate of 96Mbps.

Table 4-2 Comparison between prior works

Work	[44]	[45]	[46]	[47]	This Work
Modulation	ASK	16-QAM	4-PAM	4-QAM	Up to 64 QAM
Frequency	FM band	915 MHz	FM band	900 MHz and 2.45 GHz	1.76 GHz
RF powered compatible	Yes	No	Yes	Yes	Yes
Bit rate	500 bps	96 Mbps	10.2 kbps	500 kbps	96 Mbps
Energy/bit	NA	15.5pJ/bit†	27.7 nJ/bit*	54fJ/bit†	21.4 fJ/bit†

*Includes power consumption of control unit. †Excludes power consumption of control unit.

4.4 Chapter Summary

This chapter presents a 1.76 GHz backscattering tag that can be powered of a 2.45 GHz RF energy harvester. A key advantage of the proposed tag over the switch-based approach is the ability to select the optimal QAM constellation through adjustment of bias voltages. The varactor and a HEMT acting in the triode region are uses for this purpose. Measurement results show the proposed tag can switch from 16-QAM to 64-QAM readily and achieves a low EVM of 1.73%

Chapter 5: Simultaneous Wireless Information and Power Transfer Using Harmonic Extraction

This chapter presents a SWIPT scheme that utilizes harmonic components generated by a power transmitter and a RF energy harvesting tag. The design procedure for each is explained and the design trade-offs are analyzed. Simulation models are used to optimize the complete system.

The proposed power transmitter includes a harmonic tuned oscillator capable of synthesizing a high-power RF signal at its fundamental frequency, $f_o = 2.4\ GHz$ and at its second harmonic, $2f_o = 4.8\ GHz$. A diplexer is used to extract these frequencies and the transmitter exhibits a 75% DC to RF efficiency while producing 4 W and 0.45 W signals at f_o and $2f_o$ respectively. The oscillator exhibits a phase noise of -128 dBc/Hz at an offset frequency of 100 kHz. The corresponding FoM was found to be 182 dB.

The tag utilizes a dual band antenna to harvest both transmitted frequencies. The tag rectifier converts the received RF energy from the base station into DC as well as uses the intermodulation products generated during rectification as a carrier signal. A low power ASK modulator and transmit antenna allow the tag to relay information back to the base station or to another tag. This concept is illustrated in figure 5-1.

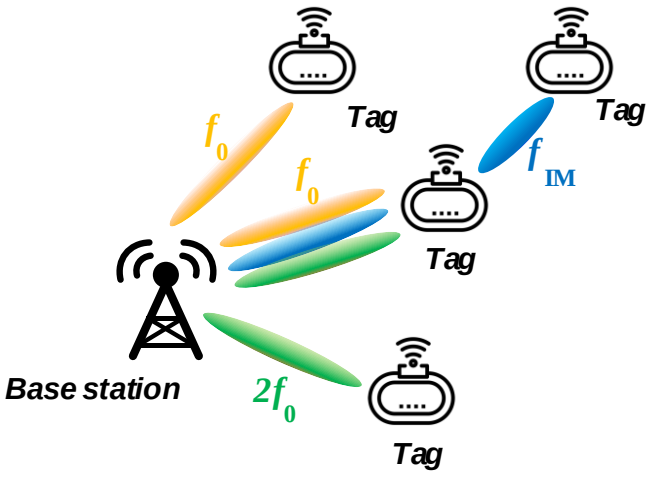

Figure 5-1: Proposed SWIPT scheme.

Section 5.1 discuss prior SWIPT methods implemented in the literature and describes their applications. Section 5.2 presents the design methodology used to optimize the transmitter overall efficiency and presents the simulation results. Similarly, Section 5.3 discusses the tag design and its performance. Section 4 concludes the chapter.

5.1 Literature Review

As explained in section 2.3.4, SWIPT systems benefit substantially using frequency duplexing as the received signal can be isolated from the transmitted signal. As a result, several publications present SWIPT systems that incorporate this method. Belo et al. developed a wireless power transmitter that uses a 5.8 GHz signal for wireless power and 3.6 GHz signal as a backscattering pilot signal [57], [58]. The tag is powered by the 5.8 GHz signal and contains a low power voltage-controlled oscillator (VCO) and mixer. These components are used to shift the received 3.6 GHz pilot signal preventing self-jamming. The system was found to be effective, but the VCO that is used to separate the base station and tag transmission frequencies requires a significant amount of power. The 3.6 GHz signal transmitted from the base station is only used for data transmission and provides no power to the energy harvester.

In another work Joseph et al. develop a SWIPT system that transmits using an amplifier and 915 MHz oscillator. [59] The tag can convert the received 915 MHz RF signal into DC with a high PCE and utilizes the second harmonic generated by the rectifier at 1.83 GHz, as a feedback signal. By having the tag generate its own carrier signal, the need for the wireless power transmitter to synthesize and broadcast at a separate frequency band to convey information was eliminated. This lowers the transmitters overall DC power consumption. However, the carrier signal generated at the tag was weak and requires a sensitive receiver at the base station. Kuo et al. also used the harmonics generated by the tags rectifier to relay a signal back to the base station [60]. Their proposed tag receives three different tones at 883 MHz, 898 MHz, and 913 MHz. All three of these frequencies are converted to DC and the intermodulation products generated are transmitted back to the base station. By receiving three different RF tones, more power can be harvested by the tag. However, the design requires that the base station contain three distinct frequency synthesizers. This consumes a significant amount of space and power.

To address the shortcomings of these works, this paper proposes a transmitter that utilizes a two-tone oscillator to synthesize a high-power RF signal at 2.4 GHz and at its second harmonic at 4.8 GHz. Figure 5-1 shows the potential application of the proposed transmitter. By transmitting two tones, the WP transmitter can provide different amounts of power to the tags, as the tags can be designed to receive a specific frequency. Tuning a tag to both transmit frequencies, f_o and $2f_o$, allows for it to receive more RF energy and the harmonic and intermodulation products from the tag's rectifier can combine to generate a higher power carrier signal at f_{IM}. The high-power carrier signal at the tag relaxes the receiver design requirements at the base station.

5.2 Dual Tone Wireless Power Transmitter Design Methodology and Performance

5.2.1 Component and Transmitter Topology Selection

GaN HEMTs are well suited for high power oscillators and amplifiers due to their high break down voltage and electron mobility, for this reason the Cree CGH 40006P RF GaN HEMT was selected for the amplification device [50] [53] [60] [61].

After selecting the amplification device, the load network was optimized to ensure a high-power output and high DC-to-RF PCE at f_o and $2f_o$ by performing a load pull simulation. The setup for the load pull is shown in figure 5-2. It is accomplished by separating the fundamental and second harmonic frequencies using a diplexer and sweeping the load impedance at each output.

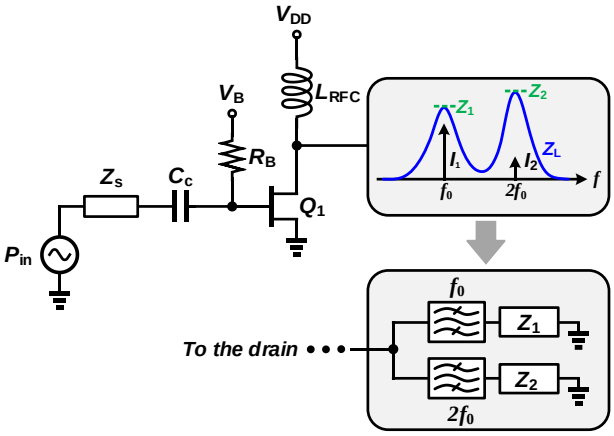

Figure 5-2: Schematic for load pull setup.

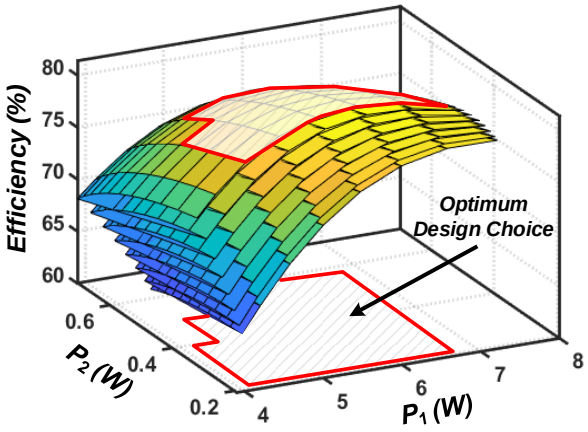

Figure 5-3: Results of load pull simulation.

The results of the load pull simulation are shown in figure 5-3. In the figure P_1 and P_2 represent the output power at f_o and $2f_o$, respectively. The efficiency is calculated using equation 28.

$$\eta = 100\% * \frac{P_1 + P_2}{P_{DC}} \tag{28}$$

5.2.2 Feedback Network Design and Diplexer Design

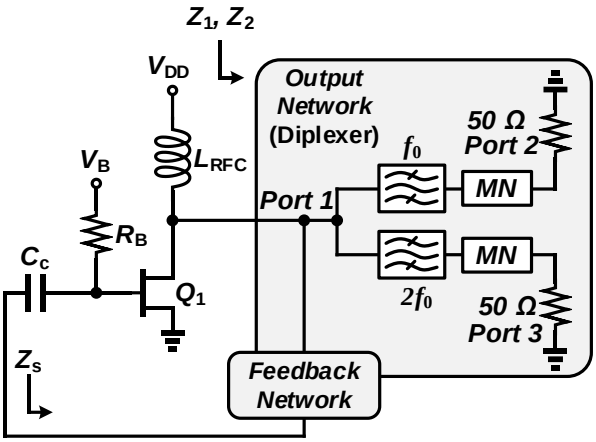

Figure 5-4: Prelimary schematic of proposed oscillator.

Figure 5-4 shows the preliminary schematic of the proposed oscillator. The oscillator scheme is modified based on the harmonic-tuned topology which has been found to achieve high efficiency at high input power levels [53] [62] [63]. The output network, the diplexer, and the feedback network, provide the required impedances at f_o and $2f_o$ to maximize the power efficiency. These impedances were determined using the load pull simulations in the previous section. The developed feedback network is shown in figure 5-5 a. and satisfies the following conditions:

1. Provide excess phase at f_o to satisfy the Barkhausen phase criteria.
2. Filter high order harmonics except for the fundamental.

The developed diplexer is shown in figure 5-5 b. and is implemented using microstrip transmission lines on Rogers 4003C. The 50-ohm terminations for ports 2 and 3 represent the antenna impedance. The diplexer is designed so that the following conditions are satisfied:

1. Maximize f_o power transferred from port 1 to port 2.
2. Maximize $2f_o$ power transferred from port 1 to port 3.
3. Isolate f_o and $2f_o$ frequency components. ($S_{32} < -20\ dB$).

Simulation results in Keysight ADS show that the loss of the diplexer is 0.45 dB and 0.6 dB at the first and second harmonics.

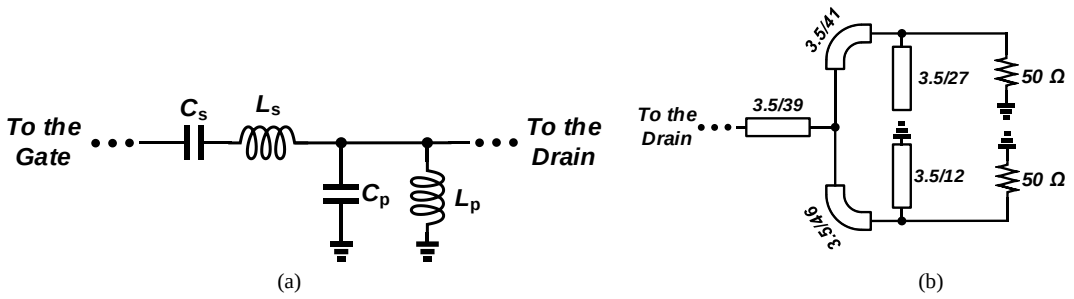

Figure 5-5: (a) Developed feedback network (b) developed diplexer.

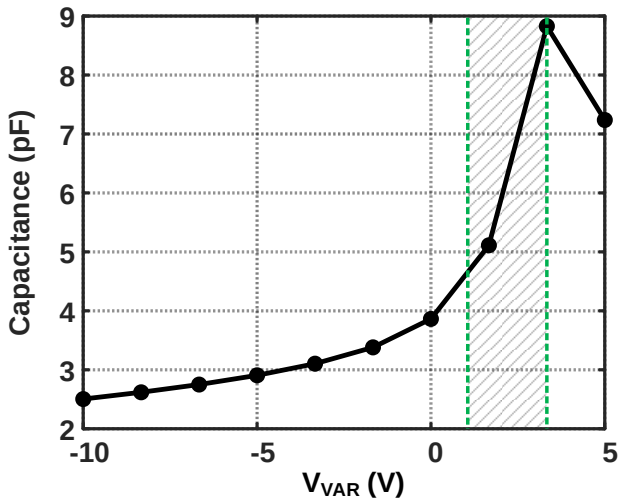

Figure 5-6: Variation of varactor capacitors for applied voltage Vvar.

5.2.3 Oscillator Tuning Range and Simulation Results

A frequency tuning mechanism was implemented to ensure the developed oscillator can achieve an oscillation frequency of 2.4 GHz despite process variations. This was achieved by connecting the drain and gate of a Cree GaN HEMT so it can act as a varactor. The variation of capacitance versus control voltage, V_{VAR}, for the Cree GaN HEMT is shown in figure 5-6 and the complete voltage-controlled oscillator design is shown in figure 5-7. A capacitance variation of 4.5 - 9.0 pF is required to achieve a tuning range of 50 MHz (≈ 2 %) around the center frequency which is translated to the control voltage range of 1-3.5 V.

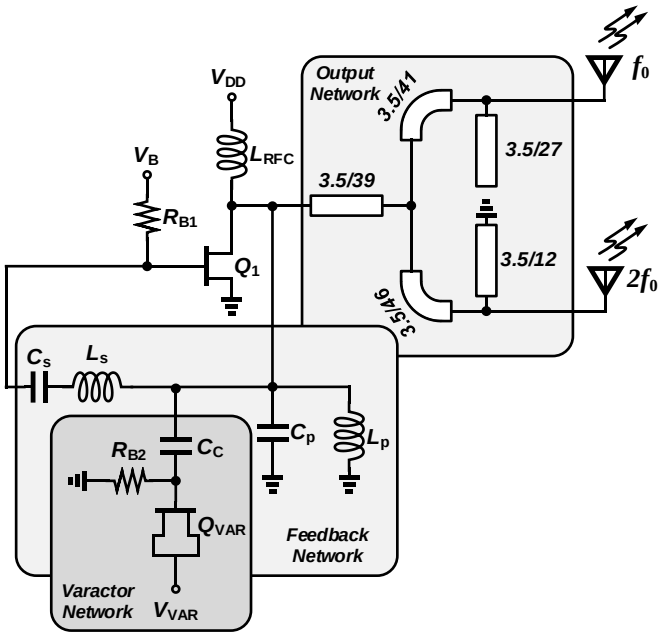

Figure 5-7: Complete schematic of proposed oscillator.

Using Keysight ADS it was found that the oscillator achieves a maximum DC to RF PCE of 75 %. This is lower than what the load pull results in section 5.2.1 indicate, which can be contributed to the loss of the diplexer. The total DC power consumption and output RF power at fundamental and second harmonics versus varactor control voltage is represented in figure 5-8. Figure 5-9 shows a plot of the oscillation frequency and RF-to-DC PCE, using the efficiency definition given in expression 28 for a given varactor control voltage.

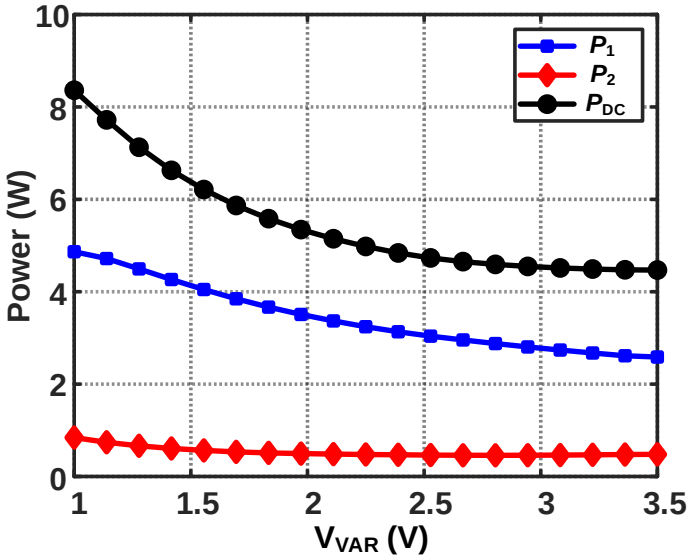

Figure 5-8: Power generation at f_o and $2f_o$.

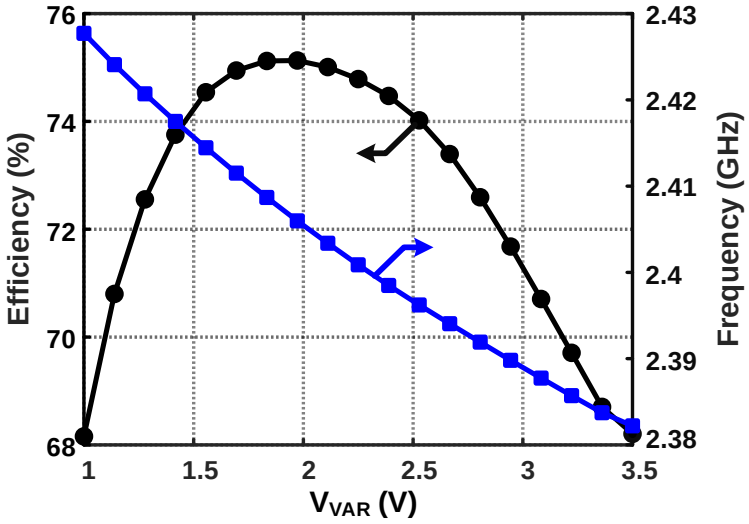

Figure 5-9: Power efficiency and fundamental frequency of the osciilation versus Vvar.

Using expressions 11 and 12, the phase noise and FoM for the oscillator design were found to be -128 dBc/Hz and 182 dB, respectively. Table 5-1 compares the performance of the proposed system to prior SWIPT and WPT works. In the table, IF frequency corresponds to the intermediate frequency that can be used to relay information. The process of generating this frequency is given in the next section.

Table 5-1: Comparision to previous works.

Work	TX Frequency (GHZ)	IF Frequency (GHZ)	TX output power (W)	TX PCE (%)	PN (dBC/Hz)	FoM (dB)
[57]	5.8	3.6	1.2	NA	NA	NA
[59]	0.915	1.83	.8	NA	NA	NA
[62]	2.45	NA	6.1	83	-118	-167
[63]	0.980	NA	6.5	73	-123	-183
This work	2.4/4.8	4.8/7.2	4/0.45	75	-128	-182

5.3 Tag Design Methodology

5.3.1 Design Constraints

The maximum distance the tag can be placed from the WPT transmitter, while still receiving sufficient power to operate continuously is constrained. It is estimated that the wireless sensor node or microcontroller for a IoT application will require at least one 1mW of power. Assuming a rectifier efficiency close to the measure results in chapter 3 ($\approx 70\%$), the tag must receive a minimum RF power of 1.42 mW. Using this received power, the f_o and $2f_o$ transmitted power from the previous section, and a typical patch antenna gain of 6 dBi, the tag range can be estimated using equation (7). This distance was found to be 2.1 meters, this corresponds to a received power of 1.51 dBm and -14 dBm at the f_o and $2f_o$, respectively. Figure 5-10 shows a plot of the received power at the two frequency bands as a function of distance. Some applications may require larger ranges, this can be accomplished by increasing transmitted power or antenna gain.

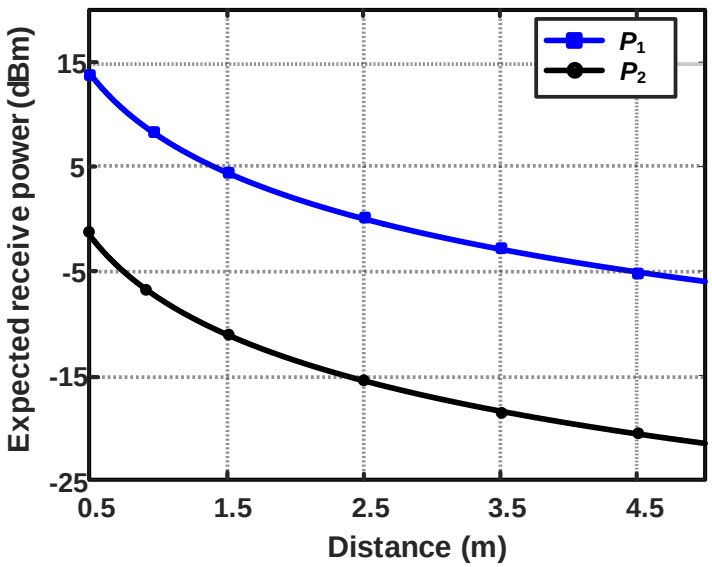

Figure 5-10: plot of at f_o (P_1) and $2f_o$ (P_2) power for a given distance.

5.3.2 Matching Network and Modulator Design

The schematic for the tag is shown in figure 5-11 with the dimensions for each impedance matching network. The first impedance matching network maximizes power transferred at f_o and $2f_o$ to the rectifier. The HSMS 2860 diode was selected for the rectifier and carrier signal generator as it was found to generate a high-power harmonic signal while maintaining a high RF-to-DC PCE [64]. The second impedance matching network is used to maximize power transferred at $3f_o$ from the carrier signal generator to the modulator. C3 is used to block DC while L1 is used to block the harmonics at the DC output and minimize ripple.

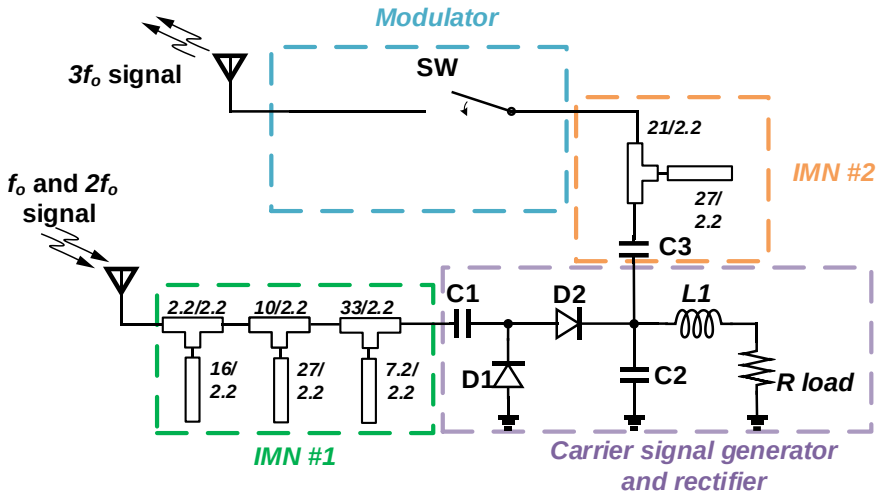

Figure 5-11: Schematic of proposed tag.

A microcontroller, powered by the rectifier, along with a switch can be used to perform ASK modulation. When the switch is closed the carrier signal $3f_o$ is transmitted conveying a '1' bit and when it is closed no signal is transmitted conveying a '0' bit. This switch can be toggled using the microcontroller and the switch can be implemented using a high frequency PIN diode such as the MA4PBL027 [65]. Figure 5-12 shows the simulation result for the ASK modulation waveform produced by the tag.

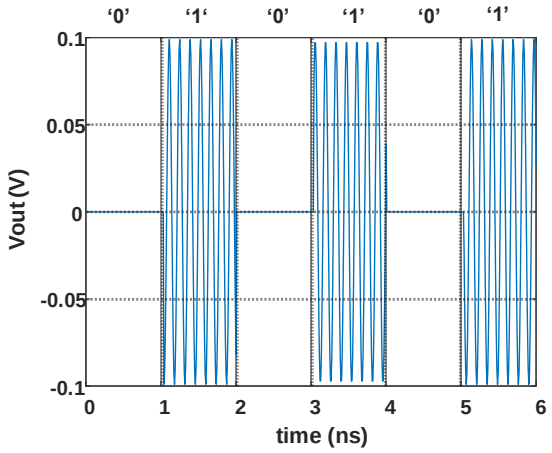

Figure 5-12: Simulation of tag modulator.

5.3.3 Simulation Results

The system shown in figure 5-11 was constructed and simulated in Keysight ADS. For a RF input power of $P_1(f_o) = 1.51\ dBm$ and $P_2(2f_o) = -14\ dBm$ the system achieved a RF-to-

DC conversion efficiency of 70 %. The RF to intermediate frequency, $f_{IM} = 7.2\ GHz$, PCE was found to be 8%. These RF-to-DC and RF-to-IF PCE were calculated by dividing the output power at 0 Hz or f_{IM} by the total input RF power. Table 5-2 compares this work to previous literature that uses harmonic signal generation and the same efficiency definitions. This work achieves a higher RF-to-IF PCE as the intermediate frequency, 7.2 GHz, corresponds to the third harmonic of the received 2.4 GHz signal as well as the intermodulation product of the 2.4 GHz and 4.8 GHz signal. The stronger IF signal allows for a higher power signal to be received at the base station, allowing for a simpler receiver design and a higher SNR.

Table 5-2 Comparision between prior works

Work	[59]	[60]	[66]	[67]	This work
# of received tones	1	3	1	2	2
Frequency (GHz)	.915	0.883,0.898,0.913	2.4	2.449,2.45	2.4,4.8
Max RF-to-DC PCE	71%	NA	70.6%	56%	70%
Max RF-to-IF PCE	1%	6%	NA	1%	8%
Harmonic feedback method	2nd	IM_3 components	3rd	$2f_2 - f_1$	3rd and $f_2 + f_1$

Simulation results show a clear design tradeoff between RF-to-DC and RF-to-IF PCE for a set input power. This tradeoff is related to the shape of the voltage waveform, V_{C_2}. V_{C_2} can be determined from performing a KCL during the positive voltage cycle and modelling the diode current using the Schottky diode formula. This is expressed in equations (29)-(31) below.

$$During\ positive\ voltage\ cycle\ i_{c_2} = i_{d_2} + i_{R_{load}}$$

$$i_{d_2} = I_s\left(e^{\frac{V_{D2}}{nV_T}} - 1\right), i_{c_2} = C_2\frac{dV_{C_2}}{dt}, i_{R_{load}} = \frac{V_{C_2}}{R_{load}} \quad (29)$$

$$C_2\ \frac{dV_{C_2}}{dt} = I_s\left(e^{\frac{V_{D2}}{nV_T}} - 1\right) + \frac{V_{C_2}}{R_{load}} \quad (30)$$

$$\therefore\ V_{C_2} - R_{load}C_2\frac{dV_{C_2}}{dt} = -R_{load}I_s(e^{\frac{V_{D2}}{nV_T}} - 1) \quad (31)$$

The solution to equation (31) can be derived by using a Taylor series expansion. However, a significant number of terms are required to accurately represent the harmonic components. A more intuitive representation of the variation in the RF-to-DC and RF-to-IF PCE is shown in figure 5-13. This figure shows the variation in each PCE for swept C_2 and R_{load} values. By changing these values, the shape of V_{C_2} waveform changes, and thus the RF-to-DC and RF-to-IF PCE values change. A value of 16kΩ and 8.8pF were selected for the load resistance and capacitance corresponding to a RF-to-DC and RF-to-IF PCE of 70% and 8%, respectively. These values were selected as it provides a reasonable IF efficiency while maintaining a high DC efficiency at the output.

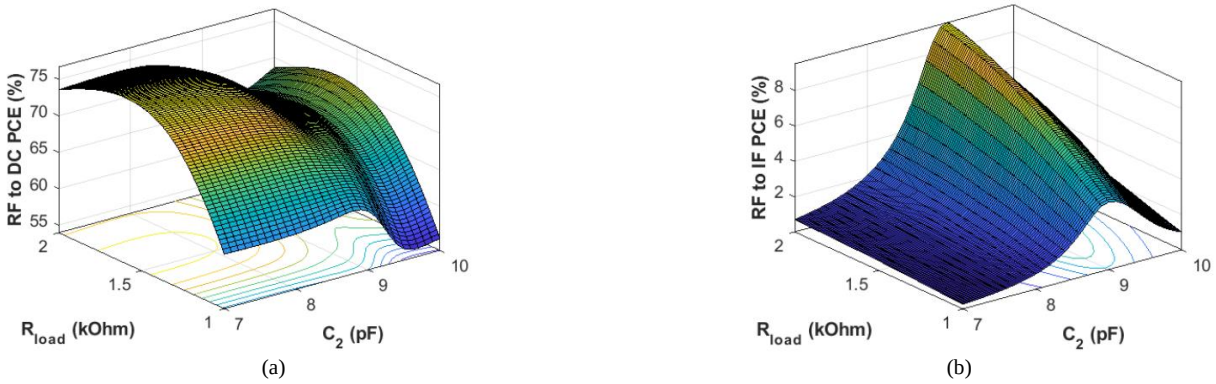

Figure 5-13: a. RF-to-DC PCE vs. R_{load} vs C_2 b. RF-to-IF PCE vs. R_{load} vs C_2

5.4 Future Work

While utilizing harmonic extraction for SWIPT enables frequency duplexing with minimal power consumption, it is spectrally inefficient. The large frequency ranges constrain applications. To address this issue, the power transmitter can be redesigned to transmit two tones with a small offset from each other, f_o and $f_o + f_{offset}$. The tag can receive these components with a wide band antenna, and then retransmit the intermodulation component shown in equation 32.

$$f_{IM} = 2(f_o + f_{offset}) - f_o = f_o + 2f_{offset} \tag{32}$$

The frequency ranges can be selected to allow the SWIPT system to operate solely in the 2.4- 2.5 GHz ISM band and avoid self-jamming. For example, if the transmit signals are 2.4 GHz

and 2.45 GHz the received signal from the tag, f_{IM}, is 2.5 GHz. A narrowband antenna with less than 50 MHz bandwidth at the receive side of the base station can strongly attenuate interference from the transmitter. Figure 5-14 illustrates the proposed SWIPT structure.

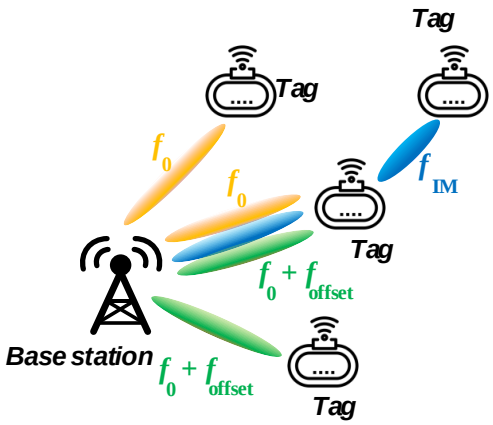

Figure 5-14: Proposed spectrally efficient SWIPT scheme.

Unlike the SWIPT scheme in section 5.2, the WPT transmitter at the base station in this scheme cannot utilize the harmonics generated by the transistor. Instead, a dual band oscillator can be constructed using a dual tank [68] [69], self-oscillating mixer [70], or injection locking structure [71]. These frequency synthesis methods have proven efficiency and exhibit low phase noise, making them well suited for SWIPT.

5.5 Chapter Summary

A SWIPT architecture consisting of a WPT transmitter and RF powered tag is designed and simulated. The advantages of using harmonic extraction for the WPT transmitter and carrier signal generation are provided. The simulation results are compared to previous works and show that the proposed tag can achieve high RF-to-DC and RF-to-IF PCE from a power efficient WPT transmitter. A new SWIPT structure that operates solely in the ISM band is also proposed.

Chapter 6: Conclusion

6.1 Summary

The efficient energy harvester and transmission methods discussed in this thesis enable the development of battery-less and large-scale communication networks, vital to implementing IoT technology. The experimental results for the RF energy harvester and backscatter modulator show that these systems have advantages over previous designs. Simulation results and analysis show the proposed SWIPT architecture also demonstrates features not developed in prior literature, such as an efficient multitone wireless power transmitter.

6.2 Key Contributions

The concepts introduced and validated in this thesis enhances SWIPT systems. The developed rectenna achieves a high RF-to-DC PCE by removing the lossy power divider. The backscatter modulator eliminates conventional fix impedance switches used in RFID systems, while maintaining a sophisticated modulation scheme using variable impedance components. The harmonic extraction SWIPT method enables higher power signals to be generated by the tag by utilizing intermodulation products from received f_o and $2f_o$ signals. An approach to designing an energy efficiency WPT is also provided.

6.3 Future Work

Several methods could be used to improve and expand upon the works presented in this thesis. To fully verify the system, the proposed oscillator and tag circuits in chapter 5 can be implemented on a PCB or IC. There are other areas where the system could be improved such as implementing beamforming, enabling multiple frequency band energy harvesting, and self-jamming cancellation mechanisms.

By implementing an antenna array and phase shifters on the WPT transmitter developed in chapter 5, the total equivalent isotropic radiated power (EIRP) can be increased. The array can be steered, based on the received signal strength of the tag signal. This would allow the tag to receive a much stronger RF signal, and thus be able to harvest a greater amount of DC energy. Implementing beamforming on a backscattering communication system or ambient energy harvester is less clear due to the power constraints but would allow for stronger RF signals to be transmitted or larger amounts of harvestable energy. Beamforming could also be implemented using intelligent reflective surfaces powered through RF energy harvesting.

The amount of harvestable energy could also be increased using multiband energy harvesting. For example, the rectenna designed in chapter 3 would have higher DC output power if it were capable of harvesting energy from DTV, cellular base stations, or other ambient RF sources in addition to the 2.4 GHz RF band. This would require multiple antennas and rectifiers or a wideband rectenna.

Self-jamming cancellation methods would allow for higher SNR, full duplex, backscattering communication. This can be done by sampling the TX signal and modifying it to cancel out the received interference. While there is not a simple method to implement this, it would allow for highly spectrally efficient communications.

References

[1] E. M. Jung et al., "A Wideband, Quasi-Isotropic, Kilometer-Range FM Energy Harvester for Perpetual IoT," in IEEE Microwave and Wireless Components Letters, vol. 30, no. 2, pp. 201-204, Feb. 2020.

[2] S. Daskalakis, A. Georgiadis, A. Bletsas and C. Kalialakis, "Dual band RF harvesting with low-cost lossy substrate for low-power supply system," 2016 10th European Conference on Antennas and Propagation (EuCAP), Davos, Switzerland, pp. 1-4, 2016.

[3] N. Shariati, W. S. T. Rowe and K. Ghorbani, "Highly sensitive FM frequency scavenger integrated in building materials," 2015 European Microwave Conference (EuMC), Paris, France, 2015, pp. 68-71

[4] M. Piñuela, P. D. Mitcheson and S. Lucyszyn, "Ambient RF Energy Harvesting in Urban and Semi-Urban Environments," in IEEE Transactions on Microwave Theory and Techniques, vol. 61, no. 7, pp. 2715-2726, July 2013.

[5] S. Keyrouz, H. J. Visser and A. G. Tijhuis, "Ambient RF energy harvesting from DTV stations," 2012 Loughborough Antennas & Propagation Conference (LAPC), Loughborough, UK, , pp. 1-4, 2012.

[6] C. Song et al., "A Novel Six-Band Dual CP Rectenna Using Improved Impedance Matching Technique for Ambient RF Energy Harvesting," in IEEE Transactions on Antennas and Propagation, vol. 64, no. 7, pp. 3160-3171, July 2016.

[7] S. Shen, Y. Zhang, C. Chiu and R. Murch, "An Ambient RF Energy Harvesting System Where the Number of Antenna Ports is Dependent on Frequency," in IEEE Transactions on Microwave Theory and Techniques, vol. 67, no. 9, pp. 3821-3832, Sept. 2019.

[8] H. Tafekirt, J. Pelegri-Sebastia, A. Bouajaj and B. M. Reda, "A Sensitive Triple-Band Rectifier for Energy Harvesting Applications," in IEEE Access,vol.8, pp. 73659-73664, 2020.

[9] U. Muncuk, K. Alemdar, J. D. Sarode and K. R. Chowdhury, "Multiband Ambient RF Energy Harvesting Circuit Design for Enabling Batteryless Sensors and IoT," in IEEE Internet of Things Journal, vol. 5, no. 4, pp. 2700-2714, Aug. 2018.

[10] K. J. P. Jimenez, J. A. Hora, O. J. L. Gerasta, X. Zhu and E. Dutkiewicz, "Self-Biased 2.4 GHz CMOS RF-to-DC Converter with 80% Efficiency and −22.04 dBm Sensitivity for Wi-Fi Energy Harvesting," 2019 IEEE International Circuits and Systems Symposium (ICSyS), Kuantan, Pahang,Malaysia, pp. 1-4, 2019.

[11] E. V. V. Cambero, H. P. da Paz, V. S. da Silva, H. X. de Araújo, I. R. S. Casella and C. E. Capovilla, "A 2.4 GHz Rectenna Based on a Solar Cell Antenna Array," in IEEE Antennas and Wireless Propagation Letters, vol. 18, no. 12, pp. 2716-2720, Dec. 2019.

[12] K. R. Sadagopan, J. Kang, Y. Ramadass and A. Natarajan, "A cm-Scale 2.4-GHz Wireless Energy Harvester With NanoWatt Boost Converter and Antenna-Rectifier Resonance for WiFi Powering of Sensor Nodes," in IEEE Journal of Solid-State Circuits, vol. 53, no. 12, pp. 3396-3406, Dec. 2018.

[13] K. Han and K. Huang, "Wirelessly Powered Backscatter Communication Networks: Modeling, Coverage, and Capacity," in IEEE Transactions on Wireless Communications, vol. 16, no. 4, pp. 2548-2561, April 2017

[14] K. Huang and V. K. N. Lau, "Enabling Wireless Power Transfer in Cellular Networks: Architecture, Modeling and Deployment," in *IEEE Transactions on Wireless Communications*, vol. 13, no. 2, pp. 902-912, February 2014

[15] Pozar, David M. Microwave Engineering. Hoboken, NJ :Wiley, 2012.

[16] S. W. Ellingson, Radio Systems Engineering (Cambridge University Press, Cambridge, England, 2016).
[17] David M. Pozar. 2000. Microwave and Rf Design of Wireless Systems (1st. ed.). Wiley Publishing.
[18] Mikeka, Chomora & Arai, Hiroyuki. (2011). Design Issues in Radio Frequency Energy Harvesting System. 10.5772/25348.
[19] ETSI, Digital cellular telecommunications system (Phase 2+); Radio transmission and reception 1996
[20] U. Olgun, C. Chen and J. L. Volakis, "Design of an efficient ambient WiFi energy harvesting system," IET Microwaves, Antennas & Propagation, vol. 6, no. 11, pp. 1200-1206, Aug. 2012
[21] M. ur Rehman, W. Ahmad and W. T. Khan, "Highly efficient dual band 2.45/5.85 GHz rectifier for RF energy harvesting applications in ISM band," 2017 IEEE Asia Pacific Microwave Conference (APMC), Kuala Lumpar, pp. 150-153, Nov. 2017.
[22] A. Hajimiri and T. H. Lee, “A general theory of phase noise in electrical oscillators,” IEEE Journal of Solid-State Circuits, vol. 33, no. 2, pp. 179–194, 1998.
[23] P. Kinget, Integrated GHz Voltage Controlled Oscillators. Boston, MA: Springer US, 1999, pp. 353–381.
[24] N. Van Huynh, D. T. Hoang, X. Lu, D. Niyato, P. Wang and D. I. Kim, "Ambient Backscatter Communications: A Contemporary Survey," in IEEE Communications Surveys & Tutorials, vol. 20, no. 4, pp. 2889-2922, Fourthquarter 2018
[25] D. T. Hoang, D. Niyato, D. I. Kim, N. V. Huynh, and S. Gong, Ambient Backscatter Communication Networks. Cambridge: Cambridge University Press, 2020.
[26] S. Daskalakis, J. Kimionis, A. Collado, M. M. Tentzeris and A. Georgiadis, "Ambient FM backscattering for smart agricultural monitoring," 2017 IEEE MTT-S International Microwave Symposium (IMS), Honololu, HI, pp. 1339-1341, 2017.
[27] S. J. Thomas and M. S. Reynolds, "A 96 Mbit/sec, 15.5 pJ/bit 16-QAM modulator for UHF backscatter communication," 2012 IEEE International Conference on RFID (RFID), pp. 185-190. Orlando, FL, 2012.
[28] S. N. Daskalakis, R. Correia, G. Goussetis, M. M. Tentzeris, N. B. Carvalho and A. Georgiadis, "Four-PAM Modulation of Ambient FM Backscattering for Spectrally Efficient Low-Power Applications," in IEEE Transactions on Microwave Theory and Techniques, vol. 66, no. 12, pp. 5909-5921, Dec. 2018.
[29] Correia and N. B. Carvalho, "Dual-Band High Order Modulation Ambient Backscatter," 2018 IEEE/MTT-S International M
[30] K. Gumber, C. Dejous and S. Hemour, "Harmonic Reflection Amplifier for Widespread Backscatter Internet-of-Things," in IEEE Transactions on Microwave Theory and Techniques, vol. 69, no. 1, pp. 774-785, Jan. 202
[31] H. L. Lee, D. Park, J. Yu and M. Lee, "Compact Antenna Module With Optimized Tx-to-Rx Isolation for Monostatic RFID," in IEEE Microwave and Wireless Components Letters, vol. 27, no. 12, pp. 1161-1163, Dec. 2017
[32] Behzad Razavi. 2011. RF Microelectronics (2nd Edition) (Prentice Hall Communications Engineering and Emerging Technologies Series) (2nd. ed.). Prentice Hall Press, USA.
[33] A. S. Boaventura and N. B. Carvalho, "Maximizing DC power in energy harvesting circuits using multisine excitation," 2011 IEEE MTT-S International Microwave Symposium, 2011, pp. 1-4

[34] B. Clerckx and E. Bayguzina, "Waveform Design for Wireless Power Transfer," in *IEEE Transactions on Signal Processing*, vol. 64, no. 23, pp. 6313-6328, 1 Dec.1, 2016
[35] G. Andia Vera, A. Georgiadis, A. Collado, and S. Via, "Design of a 2.45 GHz rectenna for electromagnetic (EM) energy scavenging," 2010 IEEE Radio and Wireless Symposium (RWS), New Orleans, LA, pp. 61-64, Jan 2010.
[36] U. Olgun, C. Chen and J. L. Volakis, "Investigation of rectenna array configurations for enhanced RF power harvesting," IEEE Antennas and Wireless Propagation Letters, vol. 10, pp. 262-265, Apr. 2011.
[37] F. Alneyadi, M. Alkaabi, S. Alketbi, S. Hajraf and R. Ramzan, "2.4GHz WLAN RF energy harvester for passive indoor sensor nodes," 2014 IEEE International Conference on Semiconductor Electronics (ICSE2014), Kuala Lumpur, pp. 471-474, Aug. 2014.
[38] H. Tafekirt, J. Pelegri-Sebastia, A. Bouajaj and B. M. Reda, "A Sensitive Triple-Band Rectifier for Energy Harvesting Applications," IEEE Access, vol. 8, pp. 73659-73664, Apr. 2020.
[39] P. Subbulakshmi and R. Rajkumar, "Design and characterization of corporate feed rectangular microstrip patch array antenna," *2013 IEEE International Conference ON Emerging Trends in Computing, Communication and Nanotechnology (ICECCN)*, 2013, pp. 547-552
[40] Balanis, Constantine A. *Antenna Theory: Analysis and Design*. 3rd ed. John Wiley, 2005.
[41] V. Kuhn, C. Lahuec, F. Seguin and C. Person, "A Multi-Band Stacked RF Energy Harvester With RF-to-DC Efficiency Up to 84%," in *IEEE Transactions on Microwave Theory and Techniques*, vol. 63, no. 5, pp. 1768-1778, May 2015
[42] Skyworks Inc., " Surface-Mount Mixer and Detector Schottky Diodes, SMS7630 series," Skyworks Datasheet, 2019.
[43] R. Corp., "RO4000 Series High Freuqnecy Circuit Materials," Rogers Datassheet, 2018.
[44] S. Daskalakis, J. Kimionis, A. Collado, M. M. Tentzeris and A. Georgiadis, "Ambient FM backscattering for smart agricultural monitoring," 2017 IEEE MTT-S International Microwave Symposium (IMS), Honololu, HI, pp. 1339-1341, 2017.
[45] S. J. Thomas and M. S. Reynolds, "A 96 Mbit/sec, 15.5 pJ/bit 16-QAM modulator for UHF backscatter communication," 2012 IEEE International Conference on RFID (RFID), pp. 185-190. Orlando, FL, 2012.
[46] S. N. Daskalakis, R. Correia, G. Goussetis, M. M. Tentzeris, N. B. Carvalho and A. Georgiadis, "Four-PAM Modulation of Ambient FM Backscattering for Spectrally Efficient Low-Power Applications," in IEEE Transactions on Microwave Theory and Techniques, vol. 66, no. 12, pp. 5909-5921, Dec. 2018.
[47] Correia and N. B. Carvalho, "Dual-Band High Order Modulation Ambient Backscatter," 2018 IEEE/MTT-S International Microwave Symposium - IMS, Philadelphia, pp. 270-273, PA, 2018.
[48] S. Thomas and M. S. Reynolds, "QAM backscatter for passive UHF RFID tags," 2010 IEEE International Conference on RFID (IEEE RFID 2010), Orlando, FL, USA, pp. 1-3, 2010.
[49] S. J. Thomas, E. Wheeler, J. Teizer and M. S. Reynolds, "Quadrature Amplitude Modulated Backscatter in Passive and Semipassive UHF RFID Systems," in IEEE Transactions on Microwave Theory and Techniques, vol. 60, no. 4, pp. 1175-1182, April 2012.
[50] Cree Inc. "CGH40006P 6 W, RF Power GaN HEMT" in Cree Wolfspeed Datasheet, 2020. [51] Skyworks Inc., "SMVA1248-079LF: Hyperabrupt Junction Tuning Varactor," in Skyworks Datasheet, 2018.J. A. Hagerty, F. B. Helmbrecht, W. H. McCalpin, R. Zane and Z. B. Popovic.
[52] I. Angelov, K. Andersson, D. Schreurs, D. Xiao, N. Rorsman1, V. Desmaris, M. Sudow, and H. Zirath, "Large-signal modelling and comparison of AlGaN/GaN HEMTs and SiC MESFETs," in Proc. AsiaPacific Microwave Conf., 2006, pp. 279–282, Dec. 2006.

[53] S. Lee, S. Jeon and J. Jeong, "Harmonic-Tuned High Efficiency RF Oscillator Using GaN HEMTs," in IEEE Microwave and Wireless Components Letters, vol. 22, no. 6, pp. 318-320, June 2012.
[54] J. Moon, J. Lee, R. S. Pengelly, R. Baker and B. Kim, "Highly Efficient Saturated Power Amplifier," in IEEE Microwave Magazine, vol. 13, no. 1, pp. 125-131, Jan.-Feb. 2012.
[55] S. Kim, H. Kim, S. Shin, J. Kim, B. Kim and J. Choi, "Combined power oscillator using GaN HEMT," 2011 IEEE MTT-S International Microwave Symposium, Baltimore, MD, USA , pp. 1-1, 2011.
[56] Microchip Technology. "PIC16(L)F1454/5/9 datasheet," Microchip datasheet, 2014.
[57] D. Belo, D. C. Ribeiro, P. Pinho, and N. Borges Carvalho, "A selective,tracking, and power adaptive far-field wireless power transfer system,"IEEE Transactions on Microwave Theory and Techniques, vol. 67, no. 9,pp. 3856–3866, 2019.
[58] D. Belo and N. B. Carvalho, "An ook chirp spread spectrum backscatter communication system for wireless power transfer applications,"IEEETransactions on Microwave Theory and Techniques, vol. 69, no. 3, pp.1838–1845, 2021
[59] S. D. Joseph, Y. Huang, S. S. H. Hsu, A. Alieldin, and C. Song, "Second Harmonic exploitation for high-efficiency wireless power transfer using uplexing rectenna,"IEEE Transactions on Microwave Theory andTechniques, vol. 69, no. 1, pp. 482–494, 2021.
[60] N. C. Kuo and A. M. Niknejad, "Rf-powered-tag intermodulation uplinkwith three-tone transmitter for enhanced uplink power,"IEEE Journalof Radio Frequency Identification, vol. 3, no. 2, pp. 56–66, 2019
[61] T. N. Thi Do, Y. Yan, and D. Kuylenstierna, "A low phase noise w-band mmic gan hemt oscillator," in2020 IEEE Asia-Pacific Microwave Conference (APMC), 2020, pp. 113–115.
[62] J. Jeong and D. Jang, "Design technique for harmonic-tuned rf poweroscillators for high-efficiency operation,"IEEE Transactions on Indus-trial Electronics, vol. 62, no. 1, pp. 221–228, 2015.
[63] W. J. Hwang, S. W. Shin, G. W. Choi, H. J. Kim, and J. J. Choi, "High-efficiency power oscillator using harmonic-tuned matching network," in2009 IEEE MTT-S International Microwave Symposium Digest, 2009,pp. 1505–1508
[64] Avago Technologies.. "HSMS-286x Series Surface Mount Microwave Schottky Detector Diodes" Avago Datasheet, 2009.
[65] MACOM Technology Solutions, "MA4PBL027 HMIC Silicon Beamlead PIN Diode V2", Macom Datasheet
[66] H. Zhang, Y. Guo, S. Gao, Z. Zhong and W. Wu, "Exploiting Third Harmonic of Differential Charge Pump for Wireless Power Transfer Antenna Alignment," in *IEEE Microwave and Wireless Components Letters*, vol. 29, no. 1, pp. 71-73, Jan. 2019, doi: 10.1109/LMWC.2018.2882086.
[67] Y. Yang, H. Wang, H. Zhang, S. Tao and Y. Guo, "Target Localization Based on Intermodulation Feedback for Multisine Wireless Power Transmission Using a Time-Modulated Array," in *IEEE Access*, vol. 8, pp. 59169-59181, 2020, doi: 10.1109/ACCESS.2020.2982697.
[68] Z. Yang, J. Dong, B. Luo, T. Yang and Y. Liu, "Low Phase Noise Concurrent Dual-Band Oscillator Using Compact Diplexer," in *IEEE Microwave and Wireless Components Letters*, vol. 25, no. 10, pp. 672-674, Oct. 2015

[69] B. Li, Y. Liu, C. Yu and Y. Wu, "Independent Control Function for Concurrent Dual-Band VCO," in *IEEE Microwave and Wireless Components Letters*, vol. 28, no. 3, pp. 230-232, March 2018,

[68] P. Burasa, N. G. Constantin and K. Wu, "Low-Power Injection-Locked Zero-IF Self-Oscillating Mixer for High Gbit/s Data-Rate Battery-Free Active RFID Tag at Millimeter-Wave Frequencies in 65-nm CMOS," in *IEEE Transactions on Microwave Theory and Techniques*, vol. 64, no. 4, pp. 1055-1065, April 2016

[70] M. Pontón, A. Herrera and A. Suárez, "Double Functionality Concurrent Dual-Band Self-Oscillating Mixer," in IEEE Transactions on Microwave Theory and Techniques, vol. 69, no. 1, pp. 786-802, Jan. 2021

[71] B. Razavi, "A study of injection locking and pulling in oscillators," in *IEEE Journal of Solid-State Circuits*, vol. 39, no. 9, pp. 1415-1424, Sept. 2004, doi: 10.1109/JSSC.2004.831608.

w